frontiers in Earth Science

ORIGINAL RESEARCH
published: 10 July 2020
doi: 10.3389/feart.2020.00276

Combining Inorganic and Organic Carbon Stable Isotope Signatures in the Schwalbenberg Loess-Palaeosol-Sequence Near Remagen (Middle Rhine Valley, Germany)

Mathias Vinnepand[1], Peter Fischer[1], Kathryn Fitzsimmons[2], Barry Thornton[3], Sabine Fiedler[1] and Andreas Vött[1]*

[1] Institute of Geography, Johannes Gutenberg University Mainz, Mainz, Germany, [2] Research Group for Terrestrial Palaeoclimates, Max Planck Institute for Chemistry, Mainz, Germany, [3] Environmental and Biochemical Sciences Group, The James Hutton Institute, Aberdeen, United Kingdom

OPEN ACCESS

Edited by:
Annett Junginger, University of Tübingen, Germany

Reviewed by:
Andrea Zerboni, University of Milan, Italy
Igor Obreht, RWTH Aachen University, Germany

****Correspondence:***
Mathias Vinnepand
mavinnep@uni-mainz.de

Specialty section:
This article was submitted to Quaternary Science, Geomorphology and Paleoenvironment, a section of the journal Frontiers in Earth Science

Received: *31 March 2020*
Accepted: *17 June 2020*
Published: *10 July 2020*

Citation:
Vinnepand M, Fischer P, Fitzsimmons K, Thornton B, Fiedler S and Vött A (2020) Combining Inorganic and Organic Carbon Stable Isotope Signatures in the Schwalbenberg Loess-Palaeosol-Sequence Near Remagen (Middle Rhine Valley, Germany). Front. Earth Sci. 8:276. doi: 10.3389/feart.2020.00276

Western Central European Loess-Palaeosol-Sequences (LPS) provide valuable terrestrial records of palaeoenvironmental conditions, which formed in response to variability in the North Atlantic climate systems. Over the last full glacial cycle (∼130 ka), climate oscillations within these systems are best documented in deep sea- and ice cores; the responses of terrestrial systems are not yet fully understood. A better understanding of metabolism governing input and output variables of organic- and inorganic C pools is, however, crucial for investigating landscape-atmospheric feedback processes and in particularly, for understanding the formation of calcareous LPS as environmental archives. Here we quantify the contributions of primary carbonates (PC) and secondary carbonates (SC) to the overall inorganic carbon pool down a LPS at the Schwalbenberg site, based on the natural abundance ratio of stable carbon isotopes ($\delta^{13}C$) and contents of the organic- and inorganic C pools. This facilitates detailed insights into the carbonate metabolism and hence, loessification and percolation processes. PC accumulate predominantly in cold phases during periods of reduced biological activity and become leached during wetter and warmer periods contemporary with higher rates of SC re-precipitation and total organic carbon (TOC) increases due to enhanced biomass production. We find that mineral dust input is most significant during stadials, as well as toward the end of warmer interstadials, characterised by gradual cooling back to stadial conditions. Pedogenesis in the Schwalbenberg LPS kept pace with surface accumulation of mineral dust. This indicates that palaeosols are of accretionary nature, which gives raise to the idea of incorporation of former topsoils in preserved subsoil horizons. Our study decodes fundamental aspects of the link between atmospheric dust circulation and terrestrial records in western Central Europe. In addition, interdependencies between factors governing the regional moisture budged and LPS can be reconstructed in a more holistic way than before.

Keywords: Loess-Palaeosol-Sequences, stable isotopes, environmental change, OIS 3, Schwalbenberg LPS

INTRODUCTION

Terrestrial carbon pools respond to changes in climate by trapping or releasing carbon to the atmosphere (Adams and Post, 1999; von Lützow and Kögel-Knabner, 2009). Consequently, total organic carbon (TOC) and total inorganic carbon (TIC) records derived from terrestrial archives can be used for correlations with ice core data along with independent age control (Adams and Post, 1999; Hatté et al., 1999). These correlations, however, pre-require detailed understanding of formation processes of investigated archives against the background of climate and environmental changes affecting terrestrial carbon pools. In context of calcareous western European Loess-Palaeosol-Sequences (LPS), we may quantify processes involved in loess formation under cold (periglacial) climate conditions and those allowing for pedogenesis under warmer interstadial or interglacial conditions. In general, loess is defined as aeolian deposits of predominantly silt-sized mineral dust (Pécsi, 1990), which undergoes syn- and post-depositional modification to produce a characteristic "loess-like-structure"; this process is often referred to as "loessification" (Sprafke and Obreht, 2016). Many processes involved are likely to be pedogenic in nature (Kemp, 2001). In this context, the role of leaching of primary carbonates (PC) and re-precipitation of hydrogenous carbonate ions as secondary carbonates (SC) is under debate (Pécsi, 1990; Sprafke and Obreht, 2016). The quantification of PC and SC, based on the natural abundance ratio of stable carbon isotopes in TIC ($\delta^{13}C_{(TIC)}$), provides a promising tool to gain insight into the role of carbonate metabolism during loess formation and to relate this processes to the palaeoenvironmental conditions prevailing during LPS formation. In particular, this can inform us about past water percolation in loess and palaeosols (cf. Zamanian et al., 2016). Under semi-arid to arid periglacial settings, water supply is a limiting factor for plant growth (Hatté et al., 2001). The first reaction of plants to drought stress is stomatal closure in order to minimise water loss during respiration (Pirasteh-Anosheh et al., 2016), leading to reduced discrimination against heavier ^{13}C isotopes in plants using the C3 photosynthesis pathway (Farquhar et al., 1982; O'Leary, 1988). Consequently, water availability to plants can be estimated if the original isotopic composition of plants is preserved in organic matter (OM) (Hatté et al., 2001), particularly in environments with limited decomposition rates, carbon turnover and root mixing. Based on this, palaeo-precipitation has been inferred from TOC in loess (Hatté et al., 2001). However, since $\delta^{13}C_{(TIC)}$ and $\delta^{13}C_{(TOC)}$ in loess sections are sensitive to water availability being multi-causal, addressing both C pools is most promising to enable more detailed insights into palaeoenvironmental processes. Moreover, differentiation of PC and SC is crucial to set up non-biased weathering indices (Buggle et al., 2011) and to understand the role of PC enriched in mineral dust during LPS formation (Kemp, 2001). In this study, we combine TIC and TOC isotope geochemistry to produce a detailed reconstruction of past dust dynamics, pedogenic processes and surface water availability of plants in light of palaeoclimate and palaeoenvironmental changes. We compare $\delta^{13}C_{(TIC)}$ and $\delta^{13}C_{(TOC)}$ to investigate processes possibly affecting both signals for core REM 3A drilled at the Schwalbenberg site. The 26 m long core reflects palaeoenvironmental conditions during the Last Glacial Cycle (LGC) (∼130 ka) in high resolution. We aim to get detailed insights into the carbonate metabolism of the LPS to estimate the degree of loessification and PC input.

REGIONAL SETTINGS

The Schwalbenberg site is located south of Remagen in the Middle Rhine valley close to the confluence of the rivers Rhine and Ahr (cf. **Figure 1**). During the LGC, thick LPS were formed by accumulation of mineral dust, loessification and pedogenesis above fluvial deposits, so far correlated to the Lower Middle Terrace of the Rhine River (Boenigk and Frechen, 2006; Schirmer, 2012). This fluvial terrace is dedicated to the penultimate glaciation and exhibits an elevation of 79 m a.s.l. (∼ 26 m above the current channel) (Boenigk and Frechen, 2006). At the Schwalbenberg itself, several valleys incised into the plateau-like loess cover. These structures are directed toward the River Rhine and follow a course almost parallel to the River Ahr. A steep slope on the south-eastern fringe of the Schwalbenberg marks the transition from the Lower Middle Terrace to the Weichselian Lower Terraces and the Holocene flood plain. The Schwalbenberg LPS has been the subject of investigations since Bibus (1980) first described the stratigraphy of an outcrop on the southern margin of the hill. At this locality a unique number of brownish palaeosols are visible within the loess sediments. Since soils reflecting interstadial climate conditions as known from Greenland ice cores for the late OIS 3 are largely missing in Central European LPS (cp. Schirmer, 2016) the question arose, whether the soils formed autochthonous or if they were the result of reworking mechanisms (Bibus, 1980). Based on litho- and pedological evidence, complemented by sedimentological, geochemical and micro-morphological proxy-data, Schirmer (2012) and Schirmer et al. (2012) addressed the eight interstadial soils as autochthonous formations being part of an LPS which mirror-pictures the OIS 3 climate succession in terms of frequency and intensity (**Figure 1**). However, chronological control is still lacking. This OIS 3 sequence was subsequently described as the "Ahrgau Subformation" (Schirmer, 2013) comprising eight interstadial soils embedded with loess, reworked loess and Gelic Gleysols. Apart from the analyses mentioned above, a sediment core (REM 1A) has been investigated by Klasen et al. (2015) trying to develop a luminescence chronology approximately 200 m distant to the outcrop (**Figure 1**). Results suggest differences in LPS formation and/or preservation throughout OIS 2 and OIS 4, whereas the sections covering OIS 3 show comparable composition and thickness further upslope. In addition, Klasen et al. (2015) and Profe et al. (2016) conducted geochemical analyses by means of x-ray fluorescence measurements. While Klasen et al. (2015) assumed changing source areas to cause differences in luminescence behaviour, Profe et al. (2016) reconstructed weathering indices and a conceptual model including multiple sediment recycling and sorting effects. In

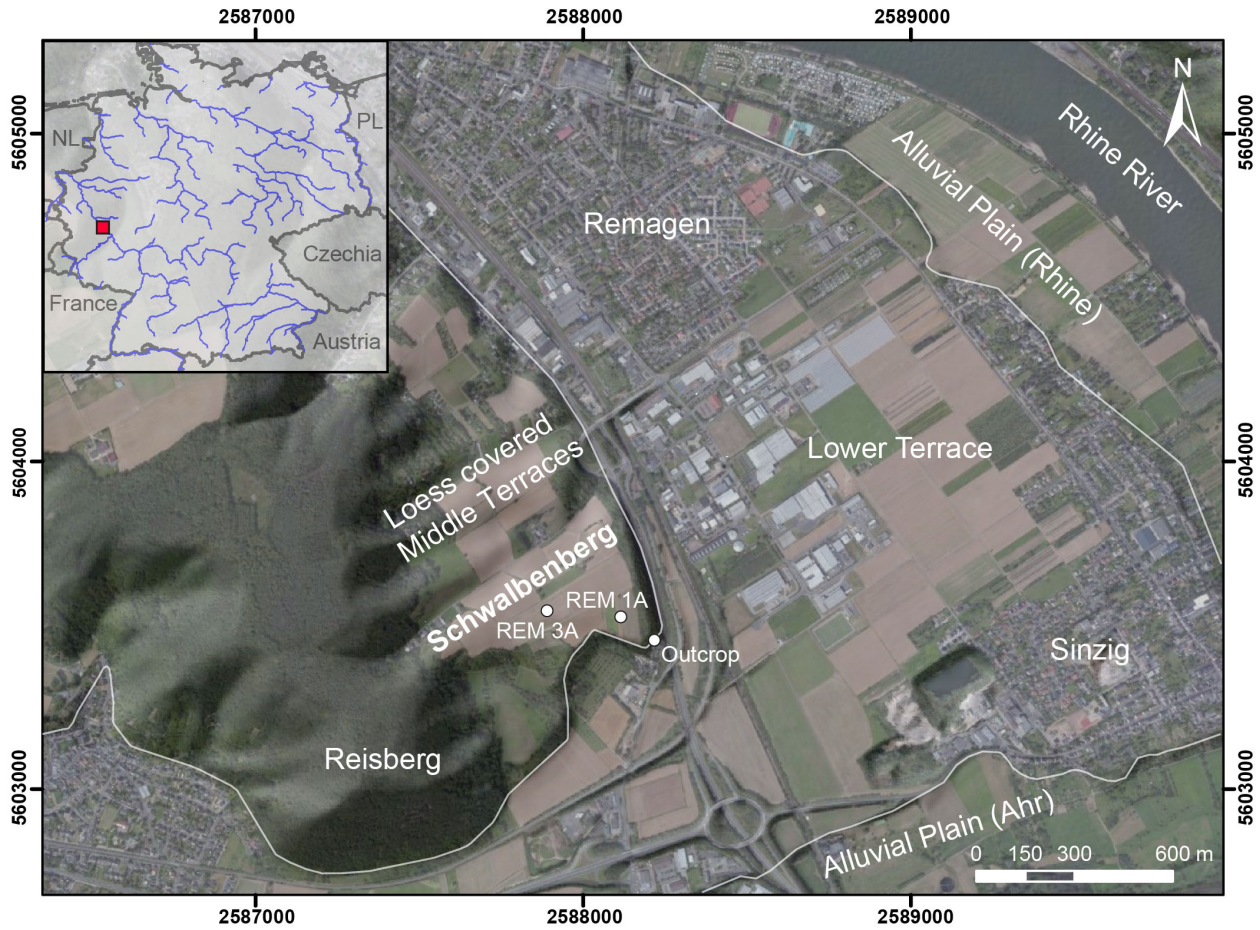

FIGURE 1 | Overview of the Schwalbenberg site in the Lower Middle Rhine Valley, Germany. The plateau-like loess relief developed on top of the Lower Middle Terrace dedicated to the penultimate glaciation (e.g., Boenigk and Frechen, 2006). Schirmer and co-workers (e.g., Schirmer, 2012; Schirmer et al., 2012) formerly investigated a 13 m thick LPS outcrop (white dot). Later on, geochemical investigations (XRF) were performed on samples derived from this outcrop by Profe et al. (2016). Sediment core (REM 1A) was obtained in mid-slope position by Klasen et al. (2015) trying to develop a luminescence chronology. The 26 m thick sediment core under investigation (REM 3A) is located in interfluve position of the Schwalbenberg.

context to this contribution, it is important to notice that Profe et al. (2016) addressed the problems of secondary calcification dynamics when applying certain element ratios. However, stable C isotope investigations have not been performed so far, which will shed new light on the formation of the Schwalbenberg LPS.

THEORETICAL BACKGROUND

During photosynthesis, plants discriminate against the heavier ^{13}C due to its lower reactivity compared to ^{12}C (Melander and Saunders, 1979). The degree of discrimination differs distinctly amongst photosynthesis pathways (O'Leary, 1981). This explains why $\delta^{13}C_{(TOC)}$ in soils and sediments is largely determined by the photosynthesis pathway under which C is sequestered in plant material (O'Leary, 1988). For the investigated Schwalbenberg LPS, the $\delta^{13}C_{(TOC)}$ are in the range of predominant C3 vegetation. Plants of this photosynthesis pathway type use the Calvin Cycle exclusively (mean −27‰ $\delta^{13}C_{VPDB}$) and dominate all forest plant communities and most plants of temperate zones (Boutton, 1996). The absence of C3/C4 vegetation shifts facilitates detailed reconstruction of carbonate metabolism without interferences. Moreover, ecological factors causing smaller isotopic fractionations like physiological water stress of plants can be addressed (Farquhar et al., 1982).

Inorganic Carbon in Loess-Palaeosol-Sequences

Three major inorganic carbon pools contribute to the overall TIC content in LPS: biogenic carbonates are formed in animals and plants as part of their skeletons or segregations (Zamanian et al., 2016; Prud'homme et al., 2018). Geogenic carbonates (PC) originate from physically weathered carbonaceous rocks within the source area of mineral dust, having $\delta^{13}C$ values close to 0‰ (West et al., 1988), and pedogenic (SC) having $\delta^{13}C$ values 14.4‰

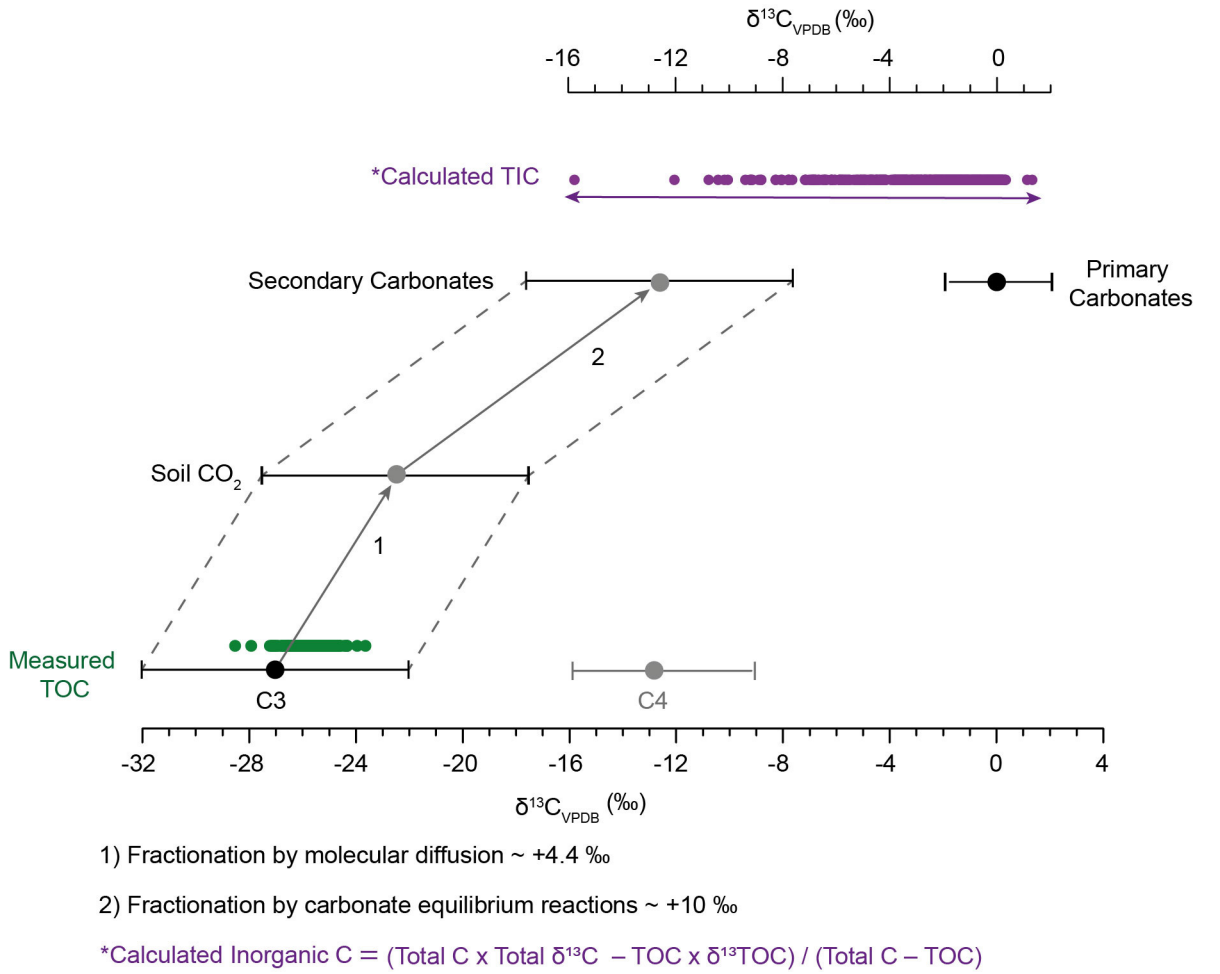

FIGURE 2 | Model of stable C isotope fractionation in calcareous terrestrial systems (redrawn from Nordt et al., 1998). Green dots represent measured $\delta^{13}C_{(TOC)}$ composition of core REM 3A. Purple dots indicate calculated δ^{13} of total inorganic C (Total C – TOC). The range of values confirms the presence of primary and secondary carbonates, which can be differentiated and quantified by end-member modelling (Salomons and Mook, 1976).

more positive than the associated OM (**Figure 2**). PC are subject to dissolution depending on contemporary climate parameters (in particular precipitation), water percolation dynamics and sediment properties (pH of the soil solution, amount of dissolved inorganic carbon through soil atmospheric CO_2 pressure pCO_2). The resulting ions are transported with soil water and precipitate as SC when the soil solution is supersaturated, in particular close to roots, in response to increasing evapotranspiration or decreasing pCO_2. Moreover, physical barriers for water percolation (e.g., related to significant decreases in particle size), may lead to accumulation of SC. Strongly decreasing pCO_2 toward the surface additionally governs the spatial distribution of SC and restricts the upward migration of ions, despite percolation of water being multidirectional (Zamanian et al., 2016). During SC precipitation, the stable carbon isotopic composition of soil CO_2 and diffusional effects determine the overall $\delta^{13}C$ values of the SC (**Figure 2**; Cerling et al., 1991). In this context, root and rhizomicrobial respiration contribute most of CO_2 in soils. Consequently, decomposition of soil organic matter (SOM) affects δ^{13} of SC only to a minor extent (Kuzyakov, 2006). Atmospheric CO_2 diffusion into soils caused by frost dynamics may shift the $\delta^{13}C$ of SC in the upper 50 cm of soils toward more positive values (Cerling, 1984). However, this is negligible in case of vegetation cover (Zamanian et al., 2016).

$\delta^{13}C$ of Total Organic Carbon ($\delta^{13}C_{(TOC)}$) in Loess

Organic carbon input to soils is mainly derived from leaf litter, root litter and exudates; faunal contribution is low (Wardle, 1992). In contrast to environments, allowing for soil formation, the TOC pool in loess is formed in relatively arid environments characterised by sparse vegetation cover, low carbon turnover rates and high mineral dust accumulation. Such environments largely restrict biases of the original isotope signal due to microbial degradation or selective preservation of recalcitrant substances and rhizosphere

disturbance (Hatté and Schwartz, 2003). The $\delta^{13}C_{(TOC)}$ in loess therefore predominantly reflects the original isotopic signal of the former vegetation ($\delta^{13}C$ of plants ($\delta^{13}C_{(PL)}$).

The following presumptions are commonly applied, when interpreting $\delta^{13}C_{(PL)}$ of C3 plants: variation in atmospheric $\delta^{13}CO_2$ has a direct impact on $\delta^{13}C_{(PL)}$, since atmospheric CO_2 forms the substrate for photosynthesis (Farquhar et al., 1989). The effect of varying atmospheric CO_2 concentration on $\delta^{13}C_{(PL)}$, has been investigated by several authors, who found a linear response of $\delta^{13}C_{(PL)}$ ($-0.02‰$ ppm^{-1} CO_2) (e.g., Feng and Epstein, 1995). However, this relationship remains under debate (Hare et al., 2018). Environmental stress may cause different degrees of isotope fractionation between plant species, as well as intra-species variation in fractionation due to genetic predisposition or differences in nutrient supply. Organs of individual plants may exhibit different $\delta^{13}C$ values (O'Leary, 1981). In light of open landscapes under which TOC in loess has been formed, we presume few plant species (mostly grasses and mosses) to be dominant (cf. Hatté and Schwartz, 2003). This would reduce the effect in variation of isotope fractionation among plant species in the resulting $\delta^{13}C_{(PL)}$ pool. Following this premise, the C pool can be regarded as a single entity in which components show somewhat similar linear responses to environmental stress (cf. Hatté and Schwartz, 2003). Temperature-related effects on $\delta^{13}C_{(PL)}$ values are difficult to assess. Several studies indicate some limited influence of temperature; others found no influence (O'Leary, 1981). On this basis we consider temperature effects to be negligible (O'Leary, 1981; Farquhar et al., 1982). Light variation potentially effect $\delta^{13}C_{(PL)}$ but only in case of large variation, such as doubling the insolation (Yakir and Israeli, 1995). There is no evidence for solar insolation shifts being this large during the LGC (Berger and Loutre, 1991). However, differences in light intensity may reach critical degrees in dense forest ecosystems. Along with variations between $\delta^{13}CO_2$ at soil surfaces (being in particularly influenced by soil atmospheric $\delta^{13}CO_2$) and $\delta^{13}CO_2$ at the canopy level (mostly reflecting atmospheric $\delta^{13}CO_2$) (Kohn, 2010). The greatest effect on C3 $\delta^{13}C_{(PL)}$ can be explained by physiological response to water availability and thereby drought stress (Kohn, 2010) in the absence of canopy effect and under relatively constant atmospheric $\delta^{13}CO_2$. Typically, the first reaction of plants to drought is stomatal closure (Pirasteh-Anosheh et al., 2016), leading to limitation of CO_2 diffusion into plants capable of increasing $\delta^{13}C_{(PL)}$ by up to $4‰$ (Farquhar et al., 1982; Stevenson et al., 2005; Kohn, 2010). In cases where precipitation exceeds ∼1500 mm yr^{-1} (Kohn, 2010), C3 plants do not show a significant reaction in their ^{13}C discrimination intensity, since there is no need for stomata closure in response to drought stress (Kohn, 2010; Thornton et al., 2015).

TOC/N$_{(total)}$

The ratio of organic carbon and total nitrogen (TOC/N$_{(total)}$) in leaves varies between plant species and is highest in evergreen (∼50) and deciduous trees (∼20). C3 herbages yield the lowest TOC/N$_{(total)}$ values (∼16.5) (Zheng and Shangguan, 2007). Decomposition of OM implies the ingestion of TOC and its partial degassing as CO_2, but also stabilisation processes. In contrast, N is incorporated in amino acids of microorganisms. Hence, smaller TOC/N$_{(total)}$ ratio indicate enhanced decomposition in case the original elemental composition does not dominate the TOC/N$_{(total)}$ ratio, due to large variation of TOC/N$_{(total)}$ in plant species (Zech et al., 2007).

TOC/PC

A ratio which combines TOC and PC may provide a useful proxy for palaeoenvironmental conditions, since both agents respond to variability in temperature, precipitation, vegetation cover, and land surface stability. Enhanced mineral dust input associated with cold conditions and reduced vegetation cover leads to the enrichment of PC and may dilutes a weak TOC signal. Climate conditions conducive to soil formation often support vegetation cover – which increases TOC input to the soil through decomposition – coeval with decreased PC input. Enhanced precipitation and especially CO_2 input by plants and microbes to the soil leads to stronger leaching of PC; this latter factor exceeds the effects of temperature for the solubility of carbonates (Zamanian et al., 2016). Assuming that the loess parent material yields $\delta^{13}C_{(TIC)}$ values of $0‰$ potentially produces a linear bias in the calculation of PC and SC. This value has been reported for limestone (West et al., 1988) and calcareous sediments and is also supported by measured stable carbon isotopic composition of "pure" loess sections throughout the REM 3A core. Here we test the TOC/PC ratio as proxy governed by the response of geomorphological and pedogenic processes to climate oscillations.

MATERIALS AND METHODS

Drilling of sediment cores was performed using a Nordmeyer RS 0/2.3 drill rig in upslope position in order to gain a preferably complete LPS. We executed vibracoring using 1 m long closed steel augers equipped with plastic liners. After drilling, cores were opened in the laboratory, photo-documented and described based on sedimentological and pedological characteristics (Ad-hoc-Ag Boden, 2005), soil classification followed the IUSS Working Group WRB (2015). However, palaeosols can hardly be classified in an accurate manner according to available nomenclature codes as these are designed for modern soils exposed to atmospheric alterations (Nettleton et al., 1998, 2000). Consequently, these nomenclatures do not account for post-burial processes including possible destruction of key soil attributes (James et al., 1998; Zerboni et al., 2011). In light of this limitation, we apply palaeosol classification similar to the WRB classification of modern soils. One half of the core was sampled in 2.5 cm intervals. Every second sample was carefully sieved (≤2 mm), dried (50°C) and homogenised by ball milling (5 min, 450 rounds/min) for further analysis.

EA-IRMS

We determined the bulk C ($C_{(total)}$), TOC and the natural abundance ratio of stable C isotopes by performing single

sample analysis. Two international reference materials (USGS40 and USGS41) were run in duplicate with every batch of 15 samples allowing a two point normalisation procedure to be performed for $\delta^{13}C$ with the same frequency. A quality control (QC) material (top soil) was measured with each batch of 15 samples; any two consecutive 2σ failures or a single 3σ failure of this QC material triggered repeated analysis of the sample batches at either side of it. Additionally, we performed tests to establish the lower limit of the amount of carbon necessary to give stable $\delta^{13}C$ and %C values. Any sample containing less than the established lower limits was re-analysed using more material. $C_{(total)}$ and $\delta^{13}C_{(total)}$ were measured by running 5 mg sample aliquots in tin cups. Since the nitrogen content can be significantly altered by HCl pre-treatment of samples (Brodie et al., 2011), we only used N data determined from untreated sample material. TOC and $\delta^{13}C_{(TOC)}$ were determined on 8 mg of sample aliquots after removal of carbonates by treatment with 0.5 M HCl in silver cups (in-cup acidification) (Midwood and Boutton, 1998). After each acidification step, the sample aliquots were dried (50°C for several hrs). This was repeated until no fizzing of CO_2 was visible anymore under a binocular microscope. The C and $\delta^{13}C$ of $C_{(total)}$ and TOC allow for calculation of TIC and its stable C isotopic composition ($\delta^{13}C_{(TIC)}$). All analyses were performed using a Flash EA 1112 Series Elemental Analyser connected through a Conflo III to a DeltaPlus V isotope ratio mass spectrometer (all Thermo Finnigan, Bremen, Germany). The $\delta^{13}C$ isotope ratios were normalised to the VPDB scale using International Atomic Energy Agency reference materials USGS40 and USGS41 (both L-glutamic acid). The C and N contents of the samples were calculated from the area output of the mass spectrometer calibrated against a topsoil standard, which was analysed with every batch of 15 samples. Long-term precision for a QC standard (top soil) (n = 116) was total carbon 3.77% (1σ = 0.12), $\delta^{13}C$ −27.79‰ (1σ = 0.14), and nitrogen 0.27% (1σ = 0.02%). The 1σ values of N, C and its stable isotope composition reflect the error margins. Values below this threshold have not been plotted in the figures. In normal operation, the CO_2 peak derived from the carbon content of the sediment sample was diluted with helium before it entered the mass spectrometer, but for samples of small carbon content (≤400 μg C) samples remained undiluted. After each run of the acidified sample aliquots, the measured TOC was checked for large shifts in its isotopic composition indicative for the presence of remaining carbonates (Boutton, 1996). This allows for crosschecking both, the reliability of the TOC content values and the $\delta^{13}C_{(TOC)}$ composition.

Calculation of Inorganic C and Its $\delta^{13}C$ Based on EA-IRMS Results

$\delta^{13}C_{(TIC)}$ was calculated using a mass balance equation

$$\delta^{13}C_{(TIC)} = ((C_{(total)} \times \delta^{13}C_{(total)}) - (TOC \times \delta^{13}C_{(TOC)}))/ (C_{(total)} - TOC) \quad (1)$$

Relative secondary carbonate (SC) proportion was calculated according to Salomons and Mook (1976):

$$SC = ((\delta^{13}C_{(TIC)} - \text{parent material } \delta^{13}C_{(TIC)}{}^{*}) / (\delta^{13}C_{(TOC)} + 14.4‰{}^{**})) \times 100 \quad (2)$$

* parent material $\delta^{13}C_{(TIC)}$ was assumed to be 0‰ based on observed $\delta^{13}C_{(TIC)}$ values in relatively unweathered loess sections and on literature data (West et al., 1988).

** 14.4‰ coefficient for fractionation due to molecular diffusion and carbonate equilibrium reactions (Nordt et al., 1998).

$$PC = 100 - SC \quad (3)$$

PC and SC contents were subsequently related to the TIC content of the respective samples to derive the weight % of both carbonate types.

Gasbench-IRMS

In order to validate calculated TIC content and its isotopic composition, we selected and re-measured 30 samples along a prominent soil complex (12–13 m in REM 3A) clearly traceable in Ca values of the downslope section, to ensure that our measure encompasses a wide range between low and high amounts of TIC. 400–500 μg of sample material was dissolved (2 h reaction time) with concentrated phosphoric acid in He-flushed borosilicate exetainers at 72°C (Gasbench II device). Subsequently the resulting CO_2 was measured using a continuous-flow IRMS (Thermo Finnigan MAT 253). Isotope data and concentration of TIC were calibrated against the NSB-19 calibrated IVA Carrara marble. Internal precision was 1σ = 0.02‰. Calculated TIC values are highly correlated with measured TIC (r^2 = 0.94, $p > 0.0001$). The same is true for its stable C isotopic composition (r^2 = 0.92, $p > 0.0001$). We checked, if calculated TIC contents (see "Calculation of Inorganic C and Its $\delta^{13}C$ Based on EA-IRMS Results") matched directly measured TIC values derived from the same samples (see "EA-IRMS") after applying the loss-of-ignition method at 550°C for 3.5 h. No relationship between these data can be observed casting doubts on both- TOC and TIC contents derived by the loss-of-ignition method applied to calcareous sediments.

RESULTS

Litho- and Pedostratigraphy of Core REM 3A

Cores REM 3A and REM 3B were drilled in upslope position of the Schwalbenberg close to Remagen (Middle Rhine valley, Germany; 50.562243° N, 7.239667° E). We performed drilling of REM 3B to a depth of 30 m below surface (b.s.) some 50 cm distant from REM 3A to extend the 26 m long record down to the underlying fluvial sediments. However, the sequence below 26 m b.s. is decalcified. Therefore, here we restrict the core description to core REM 3A (cf. **Figure 3**). Units (B-G) refer to significant shifts in lithology (note that unit A, consisting of fluvial deposits below the LPS, as well as the lowermost part of unit B are not part

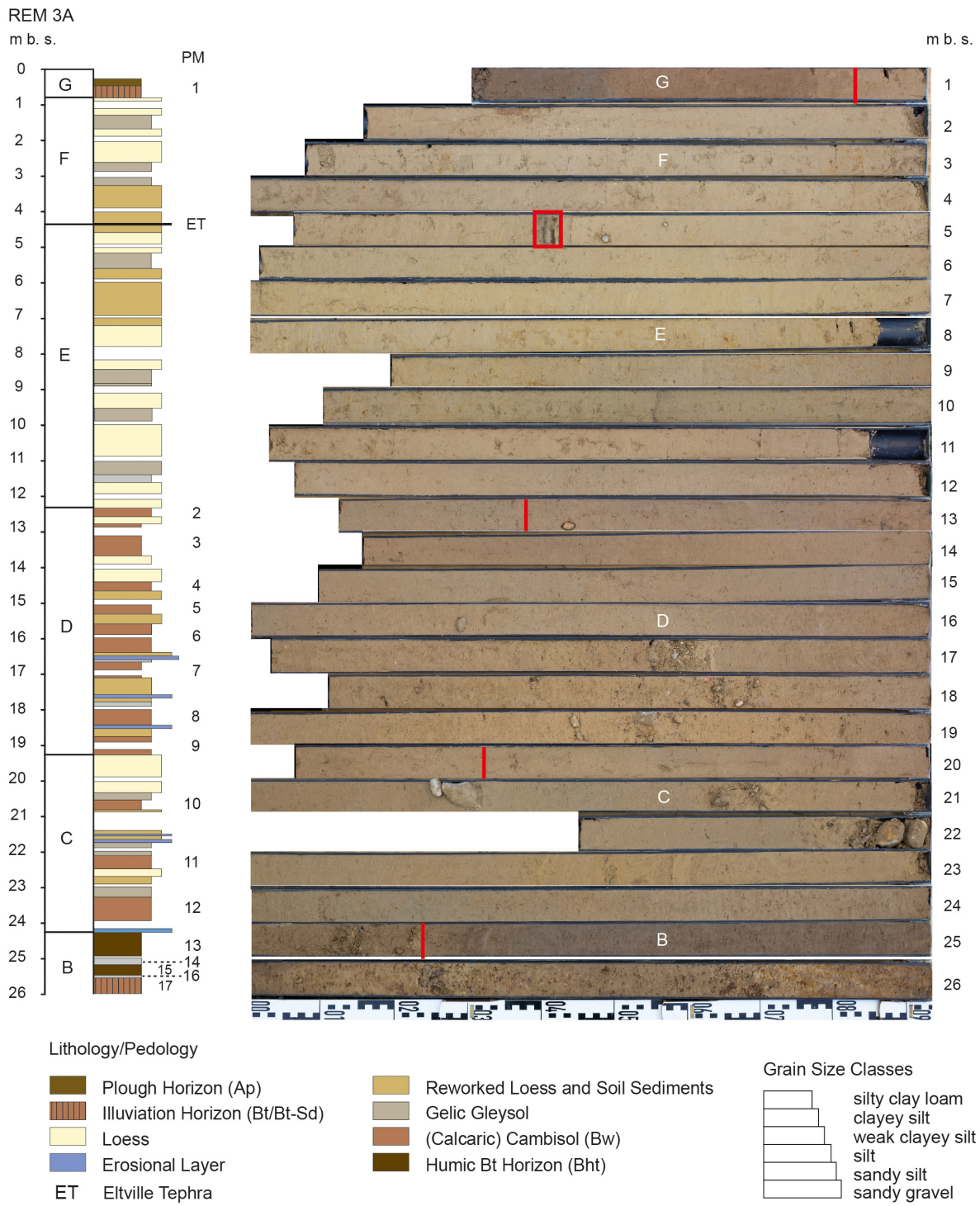

FIGURE 3 | Litho- and pedostratigraphy and photo of core REM 3A. Units B–G (indicated by red bars and white text in the photo) are described in the text (note that unit A as well as the lowermost part of unit B are not part of the core REM 3A, but REM 3B). The underlying Lower Middle Terrace of the penultimate glaciation (Boenigk and Frechen, 2006) constrains the LPS formation to the Last Glacial Cycle (terrace sediments where detected in core REM 3B, not depicted here). Soil horizons apart from Gelic Gleysols are defined as pedogenic members numbered from bottom to top (PM 1–17). Soil classification followed the IUSS Working Group WRB (2015). However, Sew and Sd horizons are based on German classification. Estimated age of the Eltville-Tephra according to Zens et al. (2017) and Förster et al. (2020).

of the core REM 3A, but REM 3B). Soil horizons apart from Gelic Gleysols are defined as pedogenic members (in the following PM) numbered from top to bottom. The lowermost unit B of the core exhibits a clayey, decalcified horizon of a truncated Stagnic Luvisol (PM 17) at its base (Sew and Sd horizons are based on German classification). It is characterised by pronounced clay cutanes followed by a leached greyish horizon (PM 16). On top of this, a weakly humic, greyish clayey horizon (PM 15) is developed. After another bleached horizon (PM 14) a dark brown, humus-enriched horizon occurs (PM 13), indicating reworking processes toward the top by intercalated layers of silt and coarse sand and a distinct erosional unconformity reflected by a gravel layer at a depth of 24.25 m b.s.. A Calcaric Cambisol (PM 12) followed by a Gelic Gleysol introduce unit C, which is characterised by reworked loess and first almost unaltered loesses (predominantly in its uppermost part). Additionally, intercalated pebbles and sand layers prove reworking processes. PM 11 contains a Calcaric Cambisol and is followed by a Gelic Gleysol characterised by carbonate pseudomycelia and an auger-filling carbonate concretion (20.27–20.32 m b.s.) indicating intensive secondary carbonate dynamics. Based on macroscopic core description the following unit D, which is characterised by a total of eight Bw horizons of Calcaric Cambisols, can be subdivided in two different parts. The lower part reaches from 18.82 up to 16.4 m b.s. and contains distinct gravel layers and reworked loess. The soil horizons (PM 9, 8, 7) show increasing intensity of pedogenic features from bottom to top. In the upper part, no more coarse-grained layers were observed. Bw horizons of Calcaric Cambisols are separated by reworked loess (PM 6, 5, 4) and loess (PM 3, 2). The thickest loess layer occurs between PM 4 and 3. Unit E is characterised by dominating yellow and grey hue values and increasing carbonate contents. Between 12.36 and 7.27 m b.s. loess sediments with intercalated Gelic Gleysols occur. This section is covered by laminated reworked loess followed by a Gelic Gleysol and another loess layer. Between 4.44 and 4.38 m b.s. the Eltville-Tephra occurs in small layers. This volcanic material is an important stratigraphic marker horizon in Western Central Europe. Klasen et al. (2015) dated the sediments below and above the tephra layer based on luminescence dating to 23.0 $\pm$ 2.3 and 21.3 $\pm$ 2.1 ka, respectively. Within the given errors, ages are in agreement with the age for the Eltville-Tephra provided by Zens et al. (2017) of 24 ka, which was recently approved by Förster et al. (2020). A comparison of the geochemical composition of the tephra from Schwalbenberg with tephra layers observed in the Auel and Dehner maar cores assumed to reflect the Eltville tephra indicate the material to be identical (personal communication Frank Sirocko). A Gelic Gleysol between 2.67 and 3.31 m marks the end of the laminated loess sections and is followed by homogeneous loess and the uppermost Gelic Gleysol. The loess on its top is characterised by numerous carbonate concretions. Unit G comprises the Holocene soil, which is represented by a truncated Luvisol.

Inorganic C and Its Stable Isotopic Composition

The decalcification line at 24.32 m marks the transition to the uppermost part of unit B which is characterised by low TIC values (**Figure 4**). Moreover, $\delta^{13}C_{(TIC)}$ curve shows a prominent trend toward more positive values. Unit C is characterised by $\delta^{13}C_{(TIC)}$ (**Figure 4**) being most negative within the lower parts of the Calcaric Cambisol (PM 12) and significantly increasing toward the following Gelic Gleysol. Unit C shows distinct maximum TIC values in the Gelic Gleysols on top of PM 11 and PM 10, respectively. High TIC values additionally occur in the reworked loess between 22.7 and 23.00 m b.s.. These maxima are accompanied by high $\delta^{13}C_{(TIC)}$ values. Minima are bound to lowest parts of Calcaric Cambisol horizons (PM 11, 10). Notably, TIC and $\delta^{13}C_{(TIC)}$ curves show decreasing values in the loess layer toward unit D. Regarding the TIC curve, in unit D all Calcaric Cambisols show lower values at their base and increasing values toward the overlying layers, only in PM 8 and PM 3 distinct minima occur. This pattern is also well reflected by $\delta^{13}C_{(TIC)}$. Reworked loess layers are associated with maximum values of $\delta^{13}C_{(TIC)}$. In contrast, unit C is characterised by less pronounced shifts in both records. Notably, minimum values of TIC occur in reworked loess layers below and above the Eltville-Tephra layer. Especially the thick laminated reworked loess between 7.27 and 5.64 m b.s. in unit E shows most positive values of $\delta^{13}C_{(TIC)}$. A second maximum is observed in a loess layer between 10 and 11 m b.s.. The uppermost part of unit F is characterised by slightly increasing TIC values and more positive $\delta^{13}C_{(TIC)}$ values.

Calculated Primary and Secondary Carbonates and Stable Isotope Signature of Total Organic Carbon ($\delta^{13}C_{(TOC)}$)

Based on an end-member-modelling approach (see "Calculation of Inorganic C and Its $\delta^{13}C$ Based on EA-IRMS Results"), we calculated the PC and SC contents using the isotopic composition of inorganic $\delta^{13}C$ (**Figures 4**, **5**). This facilitates more detailed insights into the carbonate metabolism, which is largely dependent on factors such as water availability and percolation. We also plotted the $\delta^{13}C$ curve of TOC reflecting physiological response of plants within the loess sections (Hatté et al., 1999). Focussing the palaeosols in units C and D, SC were generally enriched toward the base while PC increased in the opposite direction toward the top of the soil horizons and reached their maxima slightly above. Only within PM 8 and 2, SC showed minimum values at the base and increased values upward, the same trend was observed for PC. Distinct minima of SC and maxima of PC occurred between individual Calcaric Cambisols. In the lower part of unit E, SC are again enriched at the base of Gelic Gleysols and show absolute minima in loess and reworked loess. In unit F, SC slightly decreased from the reworked loess above the Eltville-Tephra layer toward the following Gelic Gleysol, while no clear trend was visible for the uppermost part of the unit. The same is true for PC, which increased toward the Gelic Gleysol and remained on comparably high values above. Regarding the $\delta^{13}C_{(TOC)}$ curve, a clear trend toward more positive values was observed from unit B toward the base of unit C and from the base of unit D up to the middle of unit E (7.2 m b.s.) indicating an overall decrease of water availability. Interestingly, unit C and the upper part of units E and F (above 7.2 m b.s.) are characterised by

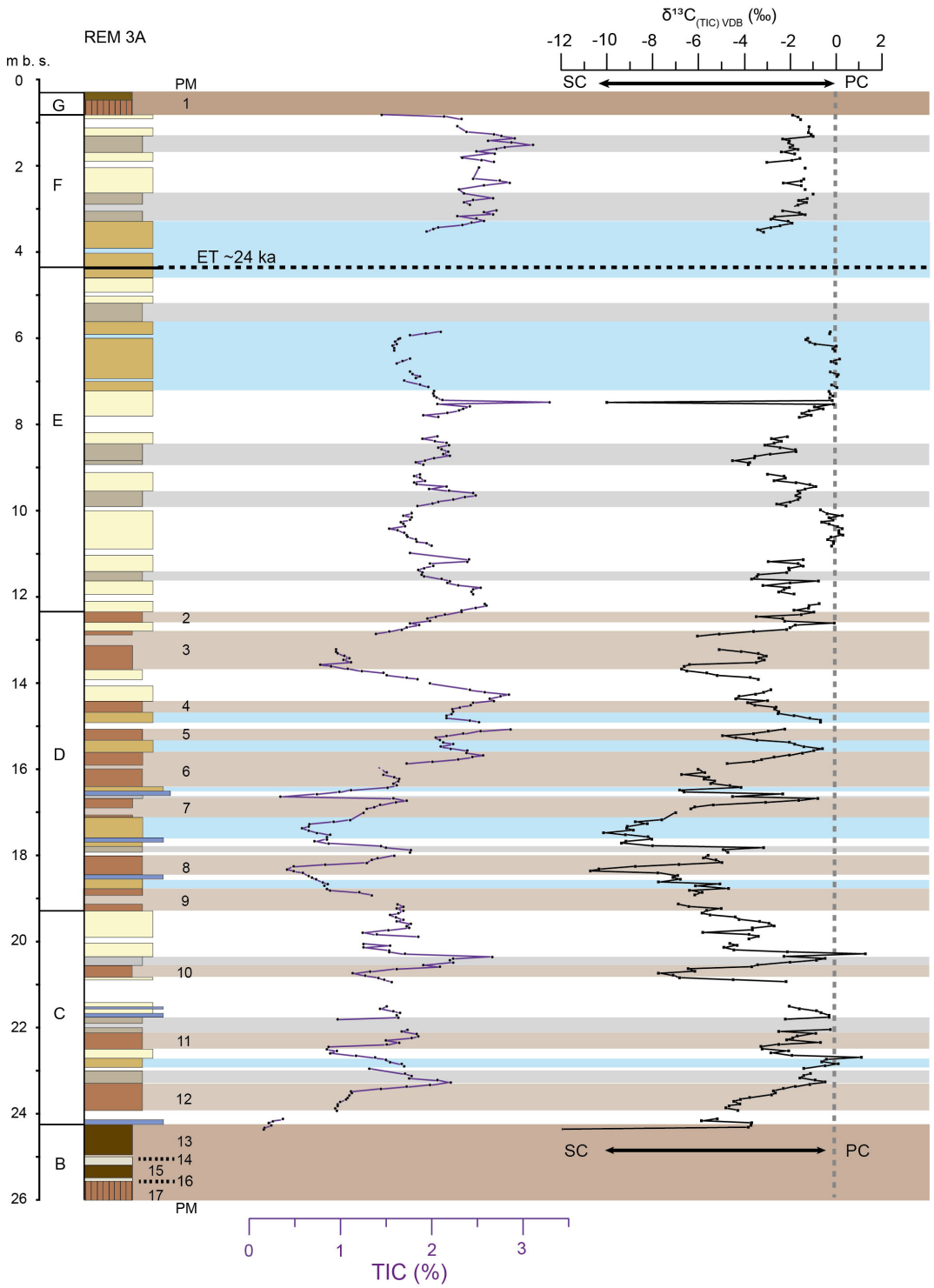

FIGURE 4 | Total inorganic C [TIC; (left, purple)] and its calculated stable C isotope composition [$\delta^{13}C_{(TIC)VPDB}$; (right, black)] where more depleted $\delta^{13}C$ values point toward enhanced SC concentration and values close to 0 indicate dominance of PC. Absolute minima in both curves are connected to pedogenic members (PM, see **Figure 3**) and occur locally in reworked loess layers (blue bars) indicating additional depletion processes. Gelic Gleysols are indicated by grey bars, Calcaric Cambisols by light brown bars and soil horizons associated with interglacial and early glacial conditions are represented by dark brown bars. Note that the lowermost part of unit (B) and the entire Holocene topsoil (A) are decalcified. Thus, no values are depicted. Estimated age of the Eltville-Tephra according to Zens et al. (2017) and Förster et al. (2020). Litho- and pedostratigraphic legend according to **Figure 3**.

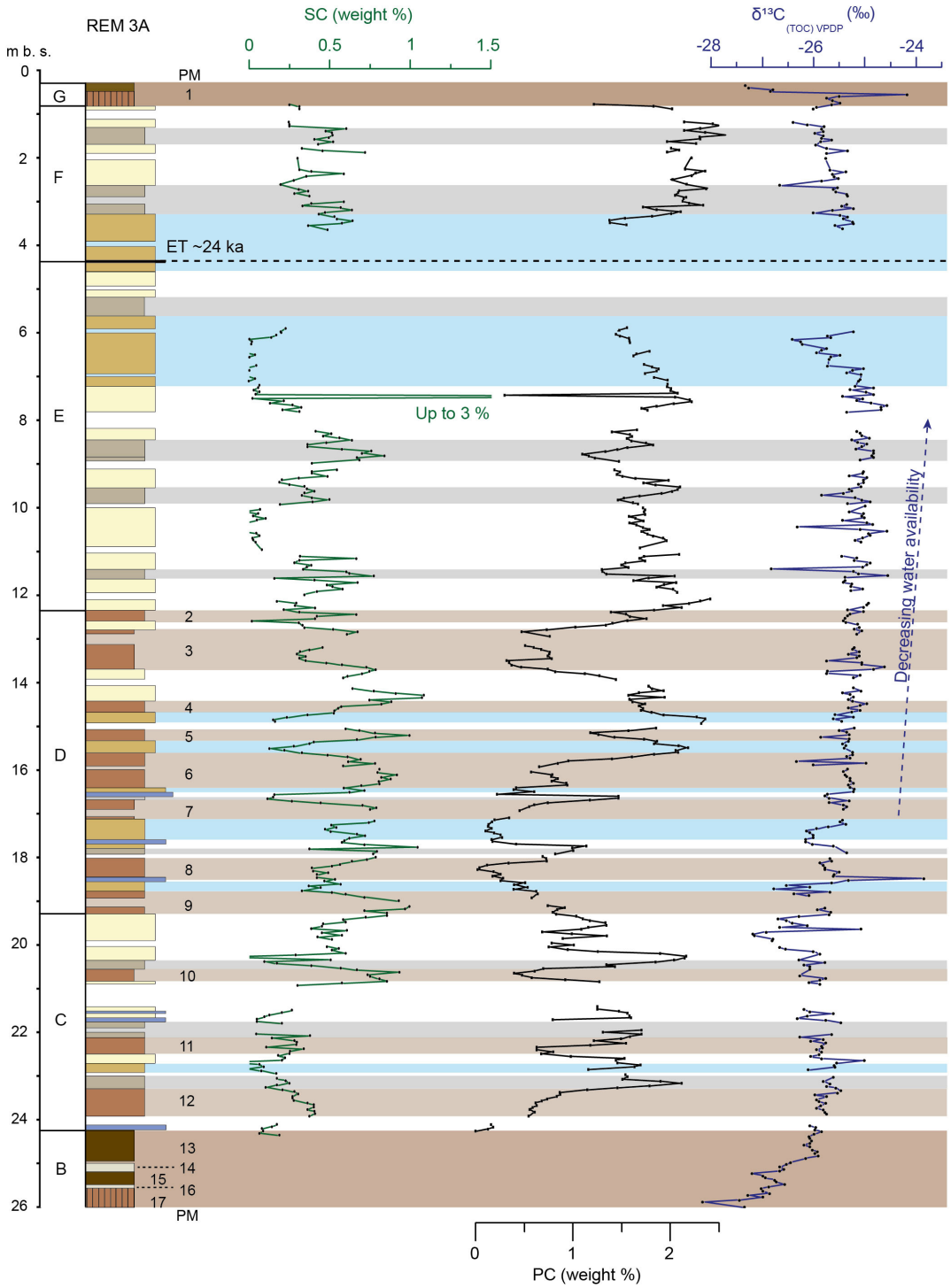

FIGURE 5 | Calculated primary and secondary carbonate contents (in weight % of TIC, see **Figure 4**) and $\delta^{13}C_{(TOC)VPDB}$. The latter reflects water availability of plants within loess and reworked loess layers, whereas in soils decomposition has to be considered (see **Figure 6**). Gelic Gleysols are indicated by grey bars, Calcaric Cambisols by light brown bars and soil horizons associated with interglacial and early glacial conditions are represented by dark brown bars. Note that the lowermost part of unit (B) and the entire Holocene topsoil (A) are decalcified. Thus, no values are depicted. Estimated age of the Eltville-Tephra according to Zens et al. (2017) and Förster et al. (2020). Litho- and pedostratigraphic legend according to **Figure 3**.

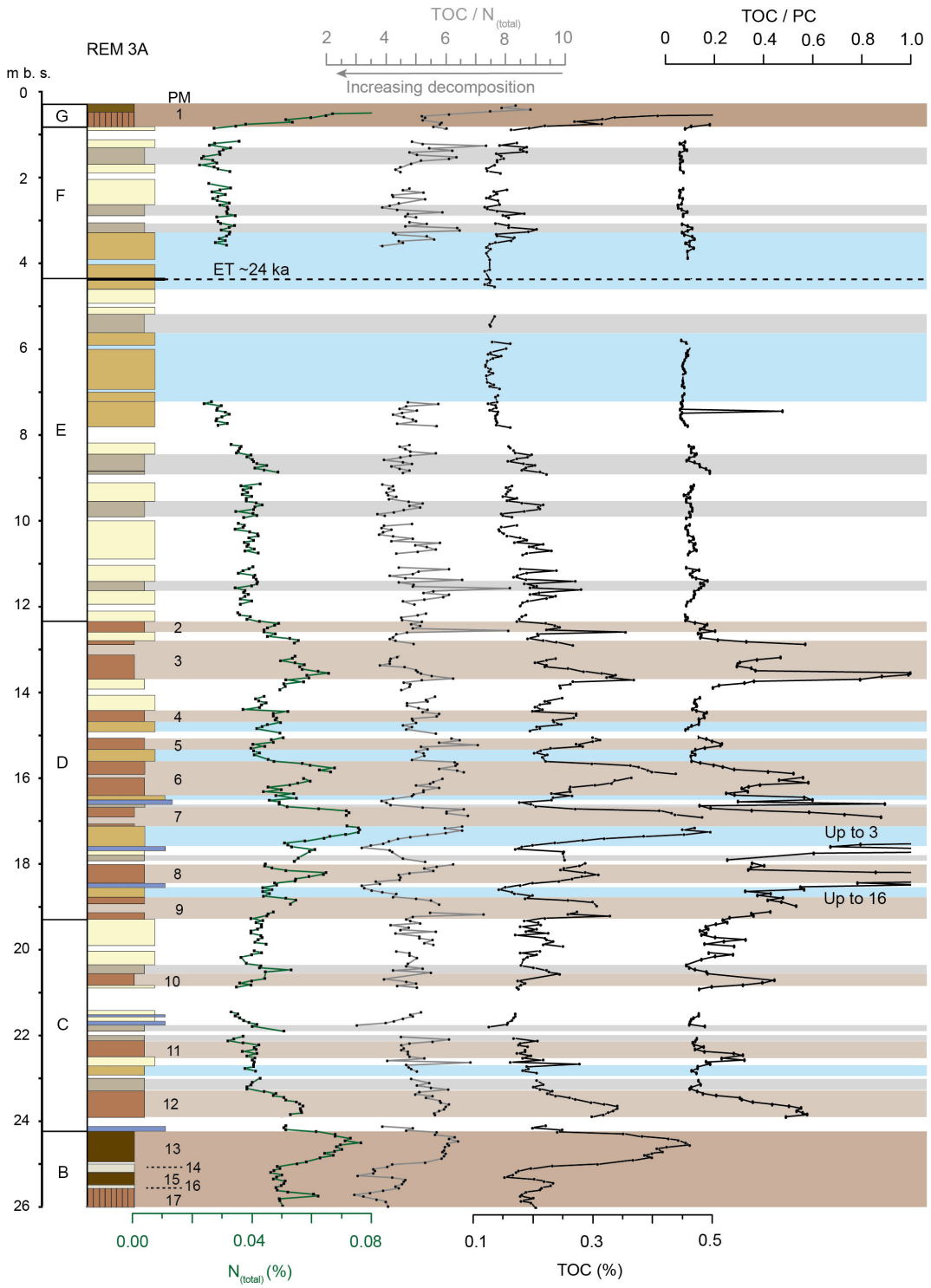

FIGURE 6 | Nitrogen ($N_{(Total)}$), total organic carbon (TOC), and their ratio (TOC/ $N_{(Total)}$) as well as the ratio of organic carbon and primary carbonates (TOC/PC) interpreted as ecological Proxies reflecting climate variability and decomposition. Values below error ranges are not depicted. Error ranges: Total *N* = 0.017%, TOC = 0.122%. Gelic Gleysols are indicated by grey bars, Calcaric Cambisols by light brown bars and soil horizons associated with interglacial and early glacial conditions are represented by dark brown bars. Note that the lowermost part of unit (B) and the entire Holocene topsoil (A) are decalcified. Thus, no values are depicted. Estimated age of the Eltville-Tephra according to Zens et al. (2017) and Förster et al. (2020). Litho- and pedostratigraphic legend according to **Figure 3**.

relatively constant values with a slight tendency toward more negative values.

Decomposition, Bioactivity and Mineral Dust Dynamics

The total nitrogen ($N_{(total)}$) and TOC contents are very low ranging between values of 0.02–0.08% and 0.05–0.5%, respectively (**Figure 6**). However, the $N_{(Total)}$, $TOC/N_{(total)}$ and TOC curves are characterised by higher values within Calcaric Cambisols compared to loess and reworked loess sections (**Figure 6**). In addition, Gelic Gleysols are characterised by enhanced TOC and $TOC/N_{(Total)}$. Distinct minima in both, $TOC/N_{(Total)}$ and TOC are related to coarse grained layers. The lowermost unit B exhibits slightly enhanced $N_{(Total)}$ values at the uppermost part of the clay enriched horizon (PM 17) of the Stagnic Luvisol. PM 16, 15, and 14 show low $N_{(Total)}$ concentration, while the humic illuviation horizon (PM 13) exhibits the highest values for $N_{(Total)}$ of the entire section. TOC values and the TOC/ $N_{(Total)}$ ratio show a slight maximum within PM 15 and a distinct maximum peak within PM 13. Apart from the Calcaric Cambisol of PM 12 characterised by maximum values in all curves, unit C is generally characterised by significantly lower values than unit B. In its lowermost part, TOC and $N_{(Total)}$ distinguish loess and reworked sediments from palaeosols. PM 11 is well reflected by the TOC/PC ratio. In contrast, the uppermost Calcaric Cambisol of unit C (PM 10) is characterised by increasing $N_{(Total)}$ and TOC values toward the top (and in the covering Gelic Gleysol). In contrast, highest TOC/PC values are located within the lowermost part in this Calcaric Cambisol (likewise for PM 11). Unit D shows a prominent saw-tooth pattern in $N_{(Total)}$ and TOC lasting from PM 7 to 4 and from 3 to 2. However, the TOC/ $N_{(Total)}$ ratio remains at a comparably high level for PMs 9 to 5. TOC/ $N_{(Total)}$ values in PMs 4, 3, and 2 are in the range of values observed in loess in the uppermost part of unit D. In contrast to all other proxies the TOC/PC ratio exhibits its highest values in PM 8. The lowermost part of this Cambisol is entirely free of PC (see also **Figure 6**). In contrast, PM 7 exhibits slightly higher, but still low PC values. PM 6 shows lowest $TOC/N_{(Total)}$ values at its bottom. In contrast, highest TOC/ $N_{(Total)}$, TOC and TOC/PC values are located at its upper part, the very top is characterised by strongly decreasing TOC and TOC/PC and TOC/ $N_{(Total)}$ being on a level as before. PM 5 exhibits most similar curve patterns for all proxies, but PM 4 is characterised by only slightly changing $N_{(Total)}$ values, whereas TOC/ $N_{(Total)}$ and TOC curve patterns are similar to those of PM 5 (but the values are lower). PM 3 exhibits maxima at its base and top and a minimum peak in-between. PM 2 is separated by a loess layer from the underlying PM 3. Strongly decreasing TOC/PC values show that the loess layer as well as PM 2 are characterised by strongly enhanced PC input. Interestingly, almost all Gelic Gleysols above the last Calcaric Cambisol of unit D are characterised by increased TOC values, whereas TOC/PC and $N_{(Total)}$ values remain low. This is, however, not true for a Gelic Gleysol from 8.50 to 9 m, which is traceable in all presented proxies.

DISCUSSION

In the following discussion we focus on presented proxy data against the background of sedimentary and pedogenic processes involved in the formation of the Schwalbenberg LPS as depicted in sediment core REM 3A. As a reliable age model is not yet available for the new core and within the Schwalbenberg II section (e.g., Schirmer, 2012; Profe et al., 2016) and only for the Sinzig Soils S2 and S3 (cp. **Figure 7**) reliable age estimates exist (App et al., 1995; Schirmer, 2012), we will briefly discuss the proxy data in context to records of global climate and environmental change of the LGC. However, we focus on the methodological approach yielding new insights into LPS formation.

Mineral Dust, Loessification and Water Dynamics

If precipitation affects calcareous mineral dust after deposition, the water would dissolve PC, which re-precipitate as SC quickly due to the surrounding alkaline environment with low bioactivity (Zamanian et al., 2016). This implies that every rainfall or melting of snow potentially leads to formation of thin SC structures capable to contributing to cementation of the sediment. In loess research much attention has been drawn on processes contributing to the "loess-like-structure" and hence cementation (Sprafke and Obreht, 2016). If relatively high quantities in SC are required to generate the loess-like structure, one would expect $\delta^{13}C_{(TIC)}$ values to be more negative similar to those observed within the "pure" loess sections in the investigated archive. In this context, one could argue that mixing of atmospheric and soil CO_2 leads to more positive values (Quade et al., 1989). We consider the role of CO_2 mixing of minor influence since we expect at least limited respiration by soil organisms and roots during phases of dust accumulation. Further potential masking of the isotopic signal could be related to input of SC received from other sites by Aeolian transport as well as differences in isotopic composition of carbonates in the source region. In this context, the heavy mineral assemblage of sediments in the study region points to the catchment area of the River Rhine as major source area (Janus, 1988). In general, the Rhine catchment mostly contains Mesozoic limestone of southern Germany and the alpine area as well as some Tertiary limestone (Brunnacker, 1983). The carbonates in theses sedimentary rocks exhibit $\delta^{13}C$ values ranging from −3 up to 2‰ $\delta^{13}C_{PDB}$ (Baertschi, 1957; Keith and Weber, 1964). Fluvial transport of PC appears to have little effect on the original isotopic composition of the carbonates. This has been shown by carbon isotope values in PC derived from overbank deposits of the Lower Terrace of the river Rhine between Koblenz and Bonn (in the vicinity of our study site) being in the range of PC in the catchment area of the river Rhine (Manze et al., 1974). More positive $\delta^{13}C_{(TIC)}$ values in the lower part of unit E (12.36–7.27 m b.s.) and in the uppermost part of unit F (3.31–0.74 m b.s.) compared to the loess layers in unit C (especially between 20.30 and 19.32 m b.s.) could be interpreted in terms of high accumulation rates under dryer climate conditions, which would

allow for rapid coverage of formerly deposited material and thus, for its protection from atmospheric processes accompanied with less SC formation. Such a scenario is also supported by relatively more positive $\delta^{13}C_{(TOC)}$ values. Overall, there is evidence for increasing aridification from OIS 3 toward OIS 2 at Nussloch in Central Europe, reflected by $\delta^{13}C$ of earthworm calcites (Prud'homme et al., 2018), $\delta^{13}C$ of TOC (Hatté et al., 1999), and grain size trends (Antoine et al., 2001). Moreover, a trend toward more positive $\delta^{13}C_{(TOC)}$ values can be observed at Achenheim (Hatté et al., 1999), but also within a transect toward SE-Europe up to the southern limit of the European loess belt in Serbia (Obreht et al., 2014). For the Belotinac section (Serbia), this trend is accompanied by increasing grain sizes (Obreht et al., 2014). Erosional unconformities, however, between PM 11 and 10, PM 9 and 8, and PM 7 and 6 are characterised by low PC and SC values indicating input of pre-weathered material. In contrast, erosional unconformities located between PM 13 and 12, and PM 8 and 7 are characterised by depleted PC but high SC values pointing toward re-precipitation of SC in response to differences in grain size. The highest overall SC concentrations are located within Calcaric Cambisols, indicating environmental conditions which allowed for PC leaching and subsequent re-precipitation. Regarding PC and SC contents in context to $\delta^{13}C_{(TOC)}$, an interpretation of $\delta^{13}C_{(TOC)}$ as proxy for palaeo-precipitation (Hatté et al., 1999, 2001) is not straightforward. This becomes obvious especially in the laminated loess layer between 7.27 and 5.64 m b.s., which is characterised by lowest SC values in the entire record. The $\delta^{13}C_{(TOC)}$ indicates moister conditions may be due to increased precipitation but could also be explained by thawing of the permafrost. At Nussloch, laminated sediments close to the Eltville-Tephra have been described to be typical for niveo-aeolian loess (Antoine et al., 2001). Niveo-aeolian loess consists of alternating snow and loess layers where the snow melts during summer periods (Pye and Tsoar, 2009). In case the permafrost-table is high, this leads to enhanced water-saturation in the active layer and allows for grain-size sorting related to fluvio-aeolian conditions (Vandenberghe, 2013). However, this may also happen without snow being embedded into the loess as melting of the uppermost centimetres of the active layer can release considerable amounts of water (Reyes and Lougheed, 2015). Therefore, water availability for plants may increase independent from precipitation, and water logging becomes progressively more significant with increasing stands of the permafrost table in response to reduced mean temperatures (cf. Fischer et al., 2017). Moreover, an increasing permafrost table would change the soil moisture flows leading to depletion of SC at the water divide and accumulation in downslope positions (Wang and Anderson, 2000). Consequently, this scenario can explain enhanced water availability indicated by $\delta^{13}C_{(TOC)}$ in loess contemporary with $\delta^{13}C_{(TIC)}$ values being close to zero during coldest phases of the LGC (**Figure 5**).

Our results indicate that "loessification" did not necessarily require enhanced quantities of SC at the Schwalbenberg site. In addition, curve patterns of both $\delta^{13}C_{(TIC)}$ and $\delta^{13}C_{(TOC)}$ indicate phases characterised by high accumulation rates under dryer climate conditions, showing that combining the isotope signatures offers considerable potential toward an understanding of past climate conditions.

Decalcification and Formation of Palaeosols

The calculated PC and SC contents in context to TIC (**Figures 5**, **7**) are interpreted to reflect carbonate metabolism along the core and thus give evidence for leaching and re-precipitation intensity within the palaeosols. TOC (**Figure 6**) is reflecting biomass production and its incorporation into the sediments and soils and increases with the duration of environmental conditions allowing for soil formation. In this context, the TOC/PC ratio (**Figure 6**) shows intensity of soil formation, when PC values decrease and TOC increase and allows tracing of dust input reflecting the accretionary character of the palaeosols within the Schwalbenberg LPS. Starting from the lowermost part of unit C, PM 12 is a well-developed soil indicated by high TOC/PC and SC values. All other Calcaric Cambisols in this unit are less pronounced in the TOC/PC but show strong influence of SC metabolism. The focus is drawn on unit D. Intensity of soil development is increasing from PM 9 over PM 8, culminating in PM 7. In the following, TOC/PC indicate decreasing development intensity over PM 6–4, while PM 3 is strongly developed again. Overall, the curve progression and its striking agreement with litho- and pedostratigraphic findings indicate a direct relation to climate oscillations during the LGC. Schirmer (2012) has already addressed the direct impact of climate oscillations on the formation of the 13 m thick Schwalbenberg II section, which is the *locus typicus* for the so called "Ahrgau-Subformation" (Schirmer, 2013). It is characterised by eight palaeosols identified as *in situ* formations reflecting climate oscillations of OIS 3 as recorded in Greenland ice cores in great detail. Based on our TIC and PC and calcium contents adapted from Profe et al. (2016), we can reliably correlate PM 5–2 of sediment core REM 3A to the upper part of the Schwalbenberg II section (Remagen Soils R4 and R5, Sinzig Soils S1–S3, **Figure 7**). As shown in **Figure 7**, PM 5 can be correlated to R4. Micro-morphological investigations of R4 indicate very low carbonate contents (Schirmer et al., 2012). However, R4 is characterised by increasing Ca-values toward its top, which is also observed in TIC and PC values of PM 5. The offset between PC and TIC in PM 5 indicate intensive SC accumulation. PM 4 correlates with R5. From a micro-morphological perspective, R5 is the most intensively developed soil of the Upper Remagen Soils (R3–R5) at the Schwalbenberg II section (Schirmer et al., 2012). TOC and maxima in the dissolved iron index identify R3 as most intense soil, which is so far not correlated to REM 3A. The lowermost part of PM 3 correlated to S1, is characterised by most depleted PC concentrations but intensive secondary carbonate precipitation (**Figures 6**, **7**). In contrast to PM 3 and the correlated S1 and S2 soils, PM 2 and S3 are developed in overall increasing alkaline environments as suggested by TIC, PC, and Ca, respectively. A high PC content is also confirmed for S3 by micro-morphological investigations (Schirmer et al., 2012). Our results show that PM 8 and the

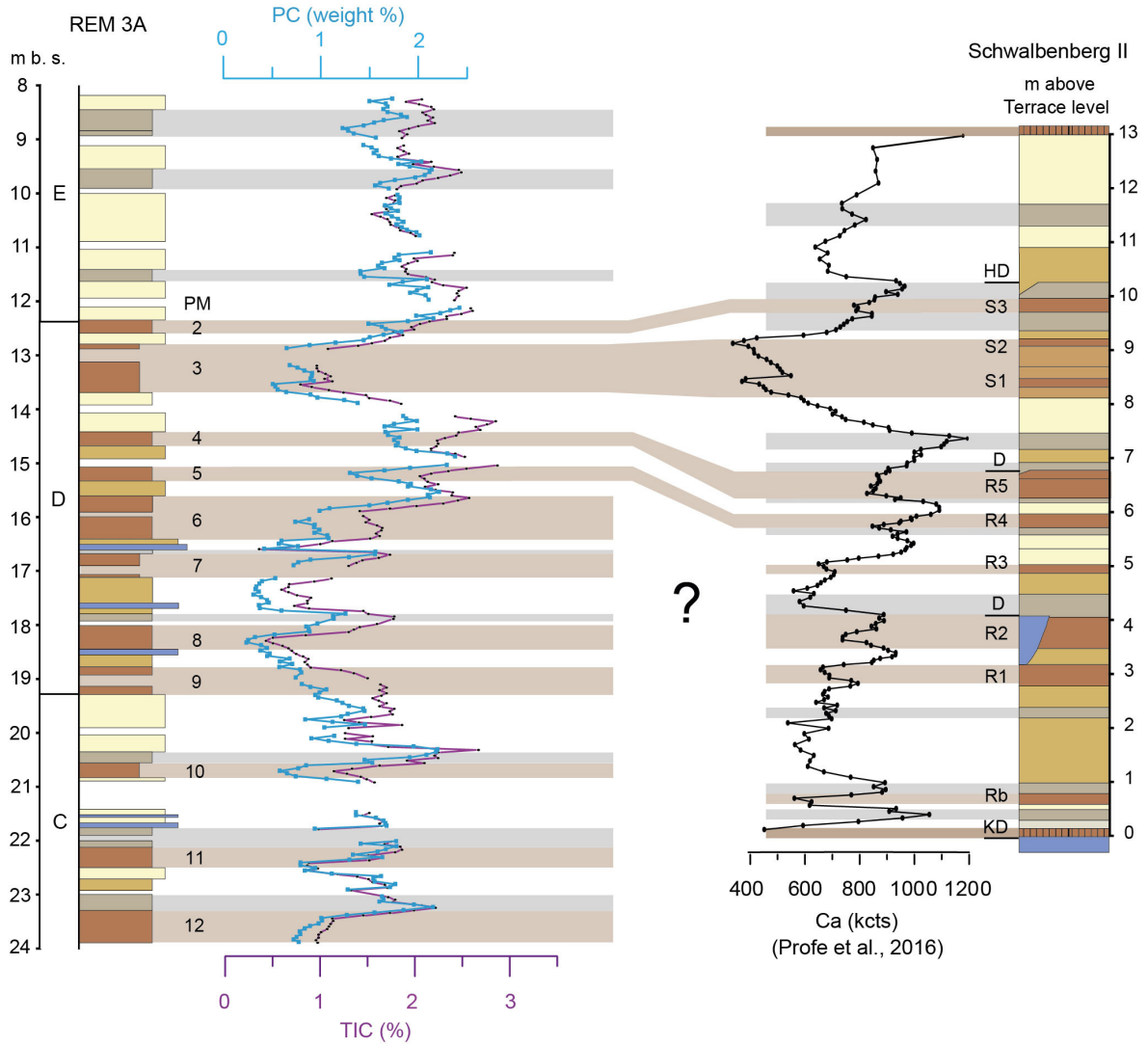

FIGURE 7 | Comparison of the TIC and Ca records and stratigraphy of the REM 3A and Schwalbenberg II section (re-drawn from Schirmer, 2012). Correlation for the uppermost parts of unit D and the Ahrgau Formation (starting above R1 up to the Hesbaye Discordance (HD)) reflecting late OIS 3 shows striking agreement amongst both LPS. However, R1 and R2 of the lower Remagen Soils and R3 of the upper Remagen Soils cannot be undoubtedly correlated to either PM (pedogenic member) 7,8,9. KD, Keldach Discordance; Rb, Reisberg Soil; D, Discordances; R1–R5, Remagen Soils; S1–S3, Sinzig Soils. Litho- and pedostratigraphic legend and pedogenic member (PM) according to **Figure 3**. Gelic Gleysols are indicated by grey bars, Calcaric Cambisols by light brown bars and soil horizons associated with interglacial and early glacial conditions are represented by dark brown bars.

lowermost part of PM 3 experienced most intensive leaching of PC amongst all Calcaric Cambisols present in REM 3A. Pronounced weathering is confirmed for the uppermost part of R1, R2, and R3 as well as for S1 and S2 by LOG (Rb/K) (Profe et al., 2016). This supports our PC results suggesting intensive leaching of most sections within the lowermost part of unit D (up to 15.50 m), which should contain the lower Remagen Soils R1 and R2 as well as R3. However, PC abundance in palaeosols appear to be inconsistent with classic concepts of soil formation, which would require complete decalcification prior to subsequent pH-dependent processes like brunification. In contrast, remarkably high PC contents are also reported for initial soil horizons toward the end of MIS 3 at the Krems-Wachtberg site (Lower Austria), where soil formation is assumed to have taken place within an alkaline environment (Meyer-Heintze et al., 2017). Based on our data, the presence of PC in a soil matrix points to an accretionary nature of most observed palaeosols in the Schwalbenberg LPS. This has also been addressed by Schirmer (2012), showing that the location of peaks in all proxies (in particularly TOC and clay content) indicates syn-pedogenetic sedimentation, at least in Remagen Soil 3 (R3). Moreover, the dissolved iron index indicates decreasing weathering toward the top of R2 and R4 (Schirmer et al., 2012).

Overall, the TOC/PC ratio proofs to be a very sensitive measure for intensity of pedogenesis at Schwalbenberg.

Correlation of Calcaric Cambisols across the slope based on PC, SC, and Ca is most promising for the Sinzig soils (S1–S3) and the upper Remagen Soils (R4–R5) (PM equivalents 5-2), but remains challenging for PM below. We relate this to differences in secondary carbonate formation and accumulation.

Decomposition

All data indicating decomposition show no general down-core trend toward enhanced degradation of TOC (**Figure 6**). This shows that long-term stabilisation constrained further decomposition of TOC (von Lützow et al., 2006; Zech et al., 2007). This is favoured by occlusion of OM into- and adsorption onto aggregates and minerals (von Lützow et al., 2006), as well as spatial inaccessibility of OM to biota (Moinet et al., 2018). TOC, $N_{(Total)}$ content and $TOC/N_{(Total)}$ show similar patterns indicating that control mechanisms of net primary production (NPP) and decomposition are largely climate dependent (Davidson and Janssens, 2006). Overall, palaeosols show distinct differences in trends of $TOC/ N_{(Total)}$. The case that $TOC/ N_{(Total)}$ values are lowest at the bottom of a soil, is the one to be expected. This is the case for PM 14, 13, 8, 6 reflecting well-developed Calcaric Cambisols most likely associated with long and warm periods of soil formation. In contrast, reverse conditions indicate erosional- and subsequent accumulation phases.

Toward a Conceptual Model of LPS Genesis

Ice core data suggest decreasing atmospheric temperature and increasing mineral dust content of the Northern Hemisphere toward the end of Greenland interstadials (GI) during OIS 3 (Ruth et al., 2003; Rasmussen et al., 2014; Rousseau et al., 2017). Since the Schwalbenberg LPS proves to be very sensitive to North Atlantic atmospheric oscillations, we hypothesise that the TOC/PC ratio is sensitive to display these atmospheric patterns. Warmer and moister interstadial periods favour pedogenesis, which starts from a stable land surface and is directed downward (Kemp, 2001). The first soil forming processes in calcareous loess involve decalcification and thus, leaching of PC. However, PC contents in REM 3A suggest an increasing input of mineral dust toward the top of palaeosols. If dust accumulation had ceased, observed clear separation of most palaeosols by calcareous loess in the Schwalbenberg LPS appears not to be plausible. We emphasise that mineral dust accumulation did not cease during formation of most interstadial soils. This implies that soils reflect the balance between mineral dust input keeping pace with soil formation. For our conceptual model, we presume the following conditions: climate warming coincides with increase of bioactivity, precipitation and decreasing mineral dust input. In turn, dust input increases as temperature and precipitation decrease. Enhanced precipitation and bioactivity during interstadials lead to increased leaching of PC and vice versa. TOC is a function of NPP and decomposition, both being largely dependent on prevailing climate. Starting from these premises the observed lowermost gradients of the TOC/PC ratio are a function of intensity and duration of pedogenesis. Climate deterioration toward the end of interstadials cause dilution of the overall TOC signal due to accumulation of PC, reflected in higher ratio values in the upper parts of palaeosols. An accretionary nature of palaeosols may also explain the absence of topsoil horizons (A-horizon) in many LPS. This common feature is often attributed to erosion due to large environmental changes at the end of interstadials/interglacials (Bronger et al., 1998). The absence of A horizons could be also explained by transformation of former A-horizons into B horizons by intercalation of illuvial components (clay and carbonates) (McDonald and Busacca, 1992; Kemp and Zárate, 2000). Such a scenario would be supported by gradually cooling and dust input toward the end of interstadials as indicated by the TOC/PC ratio. However, erosion prior to overprinting and transformation cannot be excluded. Starting from the premise that pedogenesis did not lead to complete decalcification and that the PC content of provided mineral dust did not change in order of magnitude over time, we can reconstruct pedogenetic scenarios and estimate intensity and duration of interstadials which formed the soils. Such reconstructions would require reliable age models for the Schwalbenberg LPS, which are not yet available. Only for the upper Sinzig Soils chronostratigraphic data, allowing for a correlation to certain GIs, are available. Against this background we only apply our conceptual model to the upper part of unit D. This can be extended to the entire sequence as reliable age constraints become available, contributing to a better understanding of the formation of the Schwalbenberg LPS. Sinzig Soil S2 yields an radiocarbon age of 33.350 ± 380 calBP (KIA22208, Schirmer, 2012), and Sinzig Soil S3 an age of 32.660 ± 350 calBP (KIA22209, Schirmer, 2012); App et al. (1995) give two radiocarbon ages for the archaeological find layer which corresponds to Sinzig Soil S3 yielding consistent ages of 32.480 ± 410 calBP (Pta-2722) and 32.670 ± 500 calBP (Pta-2721) [given ages were re-calibrated using the CalPal software version 2019.8 and the CalPal-2007_{HULU} (Weninger and Jöris, 2008) calibration curve]. Based on this and lithostratigraphical evidence, Schirmer (2012) correlated Sinzig Soil S2 to GI 7 and Sinzig Soil S3 to GI 6. However, S2 (correlated to the upper part of PM 3 in REM 3A) has been recently discussed to have formed during GI 6 and S3 (correlated to PM 2 in REM 3A) during GI 5 (Profe et al., 2016). GI 5 and GI 6 are characterised by rather short and less pronounced warm phases compared to previous GI 7 and in particularly GI 8 (Kindler et al., 2014; Rasmussen et al., 2014). These short and less pronounced warm phases have been discussed to be on the margin of conditions allowing for Cambisol formation (Profe et al., 2016). At the Nussloch site (∼170 km SE of Remagen), the last brown soil (Lohne Soil) has been correlated as soil complex to GI 8 and 7 and the first Gelic Gleysol (or tundra gley) is correlated to GI 6 (Moine et al., 2017).

Our results show that the lowermost part of PM 3, correlated to Sinzig Soil S1 (**Figure 7**) experienced intensive carbonate leaching and TOC accumulation (**Figures 5**, **6**). Macroscopic features indicate that this part of PM 3 is one of the most intensive palaeosols in unit D. This suggests that the lowermost part of PM 3 was formed during GI 8 rather than GI 7. The new TOC/PC ratio shows a pronounced maximum (values up to 1) in the lower part of PM 3 (**Figure 6**). In contrast, TOC/PC values decrease in

the lowermost part of PM 3. This progression is predominately governed by increasing PC toward the loess below PM 3, indicating downward leaching of carbonates in an environment with limited dust input. The strong increase of PC coinciding with a minimum in TOC/PC values at the centre of PM 3 indicate stadial conditions at the end of the GI in which Sinzig Soil S1 formed. The abruptness of PC increase may point toward conditions inhibiting strong dust input and/or preservation of PC during formation of the lowermost palaeosol. In contrast, the lower, but still relatively high TOC/PC level in the centre of PM 3 indicate loess accumulation during stadial conditions and subsequent overprinting by the overlying palaeosol (Sinzig Soil S2, upper part of PM 3). TOC/PC ratio clearly indicates that this upper part of PM 3 overprinted the underlying loess pointing to intensive pedogenesis. In this context, it is important to note that the uppermost maximum in TOC/PC is still higher than in many other Calcaric Cambisols in the core. Interestingly, the TOC/PC ratio shows a diminution toward the top of PM 2, indicating increases dust input toward the end of the GI. Overall, our results suggest that the lowermost part of PM 3 (correlated to Sinzig Soil S1) is most likely to reflect a long and warm interstadial, such as GI 8, whereas the uppermost part of PM 3 (correlated to Sinzig Soil S2) likely formed during GI 7. In this context, pollen data from maar lake archives from the Eifel area (Sirocko et al., 2016) indicate a distinct opening of the landscape in the transition from GI 8 to GI 7 characterised by a change from boreal forest (landscape evolution zone 7) to steppe conditions (landscape evolution zone 6). Our results support the idea that Sinzig Soil S3 (PM 2) reflects the last brown Calcaric Cambisol within a trend toward colder climate conditions at the margin of climates allowing for Cambisol formation (cf. Profe et al., 2016). Similar TOC/PC values within PM 2 and the first Gelic Gleysol above may render this embryonic soil as a candidate to reflect GI 5 being comparatively long and intense as GI 6 (cf. discussion Profe et al., 2016). In contrast to Nussloch at Schwalbenberg local conditions obviously allowed for later formation of one further brown soil. However, Schirmer (2012) discussed erosion of a Calcaric Cambisol in this part of the LPS. In this context, he argued that lithological properties of the Gelic Gleysol above S3 shows characteristics of the Ahrgau loess (Schirmer, 2012). We emphasis the role of factors maybe inhibiting formation of Calcaric Cambisols, but allow for Gelic Gleysols to develop. These may encompass increasing cold-arid conditions toward begin of OIS 2. Increasing aridity is indicated by progressively more positive $\delta^{13}C_{(TOC)}$ values in loess-sections at the Schwalbenberg and Nussloch sites (Hatté et al., 1999). Interestingly, our data suggest coincidentally increasing PC. Both factors are likely to directly respond to reduced temperatures (cf. Ruth et al., 2003).

Based on secure correlation of all Sinzig Soils [defined at the down-slope Schwalbenberg II section (Schirmer, 2012)] to PMs occurring at the water divide of the Schwalbenberg, no diminution of the interstadial solcomplex (OIS 3) toward upslope position can be observed, as suggested by Schirmer (2012). This is supported by geochemical investigations of the REM 1A core in mid-slope position (Klasen et al., 2015). In contrast, thickness of units reflecting the Interpleniglacial or OIS 3 appears to be consistent across the slope.

CONCLUSION AND FUTURE PERSPECTIVES

Combined investigations of TOC and TIC, as well as their stable isotope composition facilitates more detailed insights into reactions of the sedimentary and pedogenic processes to prevailing climate than addressing only one of the C pools. Hydraulic conditions governing water availability for plants can be discussed in terms of precipitation, sediment properties and permafrost dynamics in a more holistic way. In this context, we showed that enhanced water availability for plants indicated by $\delta^{13}C_{(TOC)}$ is not necessarily a function of increased precipitation but can also be caused by increased sediment moisture due to permafrost dynamics. Direct responses of terrestrial C pools to North Atlantic atmospheric and climate oscillations are likely to be reflected by the TOC/PC ratio, which is shown by a correlation of the new sediment core REM 3A to the Schwalbenberg II section. Moreover, the TOC/PC proves the accretionary nature of interstadial soils within the Schwalbenberg LPS. Beyond climatic features, we showed that cementation of mineral dust did not require high quantities of SC in the Schwalbenberg LPS, indicating that other cementation agents may play a significant role. Despite these advances, reconstructing decomposition environments and water availability for plants during time of soil formations remains difficult to assess. The main reason for this is the fact that the original isotopic signal of plants mark the starting point for further isotope fractionation during decomposition. Consequently, the resulting isotopic depth profiles can be regarded as a mixed signal including effects of water dynamics during plants lifespan, decomposition and stabilisation. Therefore, additional, investigation of compound specific $\delta^{13}C$ on recalcitrant substances like lignin is promising for isolating the effects of palaeo-precipitation and decomposition-induced changes of the isotope composition of TOC soils.

DATA AVAILABILITY STATEMENT

All datasets presented in this study are included in the article/**Supplementary Material**.

AUTHOR CONTRIBUTIONS

MV, PF, and AV wrote main parts of the manuscript. PF, AV, and KF designed the TerraClime project. BT and MV performed geochemical measurements and calculations. MV and SF conducted gasbench measurements. All authors contributed to discussion and edited the manuscript.

FUNDING

This manuscript contributes to the TerraClime Project funded by the German Research Foundation (DFG) (VO 938/25-1; FI 1941/5-1; FI 1918/4-1). BT received funding from the Rural and

Environmental Science and Analytical Services Division (RESAS) of the Scottish Government.

ACKNOWLEDGMENTS

We would like to thank Frank Sirocko for the information concerning the geochemical analysis of volcanic ash derived from the REM3 core. Moreover, constructive and valuable comments of two reviewers helped to significantly improve the manuscript.

SUPPLEMENTARY MATERIAL

The Supplementary Material for this article can be found online at: https://www.frontiersin.org/articles/10.3389/feart.2020.00276/full#supplementary-material

REFERENCES

Adams, J., and Post, W. M. (1999). A preliminary estimate of changing calcrete carbon storage on land since the Last Glacial Maximum. *Glob. Planet. Change* 20, 243–256. doi: 10.1016/s0921-8181(99)00015-6

Ad-hoc-Ag Boden (2005). Sponagel, H., Ad-hoc-Arbeitsgruppe Boden der Staatlichen Geologischen Dienste und der Bundesanstalt für Geowissenschaften und Rohstoffe, Bundesanstalt für Geowissenschaften und Rohstoffe eds Bodenkundliche Kartieranleitung: mit 103 Tabellen und 31 Listen. 5., verbesserte und erweiterte Auflage. Stuttgart: E. Schweizerbart'sche Verlagsbuchhandlung (Nägele und Obermiller).

Antoine, P., Rousseau, D. D., Zöller, L., Lang, A., Munaut, A. V., Hatté, C., et al. (2001). High-resolution record of the last Interglacial–glacial cycle in the Nussloch loess–palaeosol sequences, Upper Rhine Area, Germany. *Quat. Int.* 76–77, 211–229. doi: 10.1016/S1040-6182(00)00104-X

App, V., Auffermann, B., Hahn, J., Pasda, C., and Stephan, E. (1995). "Die altsteinzeitliche fundstelle auf dem schwalbenberg bei remagen," in *Berichte zur Archäologie an Mittelrhein und Mosel*, Vol. 4, ed. W. Wegner (Koblenz: Gesellschaft für Archäologie an Mittelrhein und Mosel), 11–27.

Baertschi, P. (1957). Messung und deutung relativer Häufigkeitsvariationen von 018 und C13 in Karbonatgesteinen und Mineralien. *Schweiz. Mineral. Petrogr. Mitt.* 87, 75–152.

Berger, A., and Loutre, M. F. (1991). Insolation values for the climate of the last 10 million years. *Quat. Sci. Rev.* 10, 297–317. doi: 10.1016/0277-3791(91)90033-Q

Bibus, E. (1980). *Zur Relief-, Boden- und Sedimententwicklung am Unteren Mittelrhein*. Frankfurt: Frankfurter Geowissenschaftliche.

Boenigk, W., and Frechen, M. (2006). The Pliocene and quaternary fluvial archives of the Rhine system. *Quat. Sci. Rev.* 25, 550–574. doi: 10.1016/j.quascirev.2005.01.018

Boutton, T. W. (1996). "Stable carbon isotope ratios of soil organic matter and their use as indicators of vegetation and climate change," in *Mass Spectrometry of Soils*, eds T. W. Boutton and S. Y. Yamasaki (New York, NY: Marcel Dekker), 47–82.

Brodie, C. R., Leng, M. J., Casford, J. S. L., Kendrick, C. P., Lloyd, J. M., Yongqiang, Z., et al. (2011). Evidence for bias in C and N concentrations and δ13C composition of terrestrial and aquatic organic materials due to pre-analysis acid preparation methods. *Chem. Geol.* 282, 67–83. doi: 10.1016/j.chemgeo.2011.01.007

Bronger, A., Winter, R., and Heinkele, T. (1998). Pleistocene climatic history of East and Central Asia based on paleopedological indicators in loess–paleosol sequences. *Catena* 34, 1–17. doi: 10.1016/s0341-8162(98)00078-2

Brunnacker, K. (1983). Isotopendaten im lößkalk der europäischen periglazialzone. *Mitt. Österrereichischen Geol. Ges.* 76, 205–211.

Buggle, B., Glaser, B., Hambach, U., Gerasimenko, N., and Markoviæ, S. (2011). An evaluation of geochemical weathering indices in loess–paleosol studies. *Quat. Int.* 240, 12–21. doi: 10.1016/j.quaint.2010.07.019

Cerling, T. E. (1984). The stable isotopic composition of modern soil carbonate and its relationship to climate. *Earth Planet. Sci. Lett.* 71, 229–240. doi: 10.1016/0012-821X(84)90089-X

Cerling, T. E., Solomon, D. K., Quade, J., and Bowman, J. R. (1991). On the isotopic composition of carbon in soil carbon dioxide. *Geochim. Cosmochim. Acta* 55, 3403–3405. doi: 10.1016/0016-7037(91)90498-T

Davidson, E. A., and Janssens, I. A. (2006). Temperature sensitivity of soil carbon decomposition and feedbacks to climate change. *Nature* 440, 165–173. doi: 10.1038/nature04514

Farquhar, G. D., Ehleringer, J. R., and Hubick, K. T. (1989). Carbon isotope discrimination and photosynthesis. *Annu. Rev. Plant Physiol. Plant Mol. Biol.* 40, 503–537. doi: 10.1146/annurev.pp.40.060189.002443

Farquhar, G. D., O'Leary, M., and Berry, J. (1982). On the relationship between carbon isotope discrimination and the intercellular carbon dioxide concentration in leaves. *Funct. Plant Biol.* 9, 121–137. doi: 10.1071/PP9820121

Feng, X., and Epstein, S. (1995). Carbon isotopes of trees from arid environments and implications for reconstructing atmospheric CO2 concentration. *Geochim. Cosmochim. Acta* 59, 2599–2608. doi: 10.1016/0016-7037(95)00152-2

Fischer, P., Hambach, U., Klasen, N., Schulte, P., Zeeden, C., Steininger, F., et al. (2017). Landscape instability at the end of MIS 3 in western Central Europe: evidence from a multi proxy study on a loess-palaeosol-sequence from the eastern lower Rhine embayment, Germany. *Quat. Int.* 502, 119–136. doi: 10.1016/j.quaint.2017.09.008

Förster, M. W., Zemlitskaya, A., Otter, L. M., Buhre, S., and Sirocko, F. (2020). Late Pleistocene Eifel eruptions: insights from clinopyroxene and glass geochemistry of Tephra layers from Eifel Laminated Sediment Archive sediment cores. *J. Quat. Sci.* 35, 186–198. doi: 10.1002/jqs.3134

Hare, V. J., Loftus, E., Jeffrey, A., and Ramsey, C. B. (2018). Atmospheric CO2 effect on stable carbon isotope composition of terrestrial fossil archives. *Nat. Commun.* 9:252. doi: 10.1038/s41467-017-02691-x

Hatté, C., Antoine, P., Fontugne, M., Lang, A., Rousseau, D. D., and Zöller, L. (2001). δ 13 C of loess organic matter as a potential proxy for paleoprecipitation. *Quat. Res.* 55, 33–38. doi: 10.1006/qres.2000.2191

Hatté, C., Fontugne, M., Rousseau, D. D., Antoine, P., Zöller, L., Tisnérat-Laborde, N., et al. (1999). δ13C variation of loess organic matter as a record of the vegetation response to climate changes during the Weichselian. *Geology* 26, 583–586.

Hatté, C., and Schwartz, D. (2003). Reconstruction of paleoclimates by isotopic analysis: what can the fossil isotopic record tell us about the plant life of past environments? *Phytochem. Rev.* 2, 163–177. doi: 10.1023/B:PHYT.0000004260.40656.c0

IUSS Working Group WRB (2015). *World Reference Base for Soil Resources 2014, Update 2015 International Soil Classification System for Naming Soils and Creating Legends for Soil Maps*. Rome: IUSS.

James, W. C., Mack, G. H., and Monger, H. C. (1998). Paleosol classification. *Quat. Int.* 51, 8–9. doi: 10.1016/s1040-6182(98)90186-0

Janus, U. (1988). *Löss der Südlichen Niederrheinischen Bucht*. Doctoral dissertation, Kölner Geographische Arbeiten, Köln.

Keith, M. L., and Weber, J. N. (1964). Carbon and oxygen isotopic composition of selected limestones and fossils. *Geochim. Cosmochim. Acta* 28, 1787–1816. doi: 10.1016/0016-7037(64)90022-5

Kemp, R. A. (2001). Pedogenic modification of loess: significance for palaeoclimatic reconstructions. *Earth Sci. Rev.* 54, 145–156. doi: 10.1016/s0012-8252(01)00045-9

Kemp, R. A., and Zárate, M. (2000). Pliocene pedosedimentary cycles in the southern Pampas, Argentina. *Sedimentology* 47, 3–14. doi: 10.1046/j.1365-3091.2000.00274.x

Kindler, P., Guillevic, M., Baumgartner, M., Schwander, J., Landais, A., and Leuenberger, M. (2014). Temperature reconstruction from 10 to 120 kyr b2k from the NGRIP ice core. *Clim. Past* 10, 887–902. doi: 10.5194/cp-10-887-2014

Klasen, N., Fischer, P., Lehmkuhl, F., and Hilgers, A. (2015). Luminescence dating of loess deposits from the Remagen-Schwalbenberg site, Western Germany. *Geochronometria* 42, 67–77.

Kohn, M. J. (2010). Carbon isotope compositions of terrestrial C3 plants as indicators of (paleo)ecology and (paleo)climate. *Proc. Natl. Acad. Sci. U.S.A.* 107, 19691–19695. doi: 10.1073/pnas.1004933107

Kuzyakov, Y. (2006). Sources of CO2 efflux from soil and review of partitioning methods. *Soil Biol. Biochem.* 38, 425–448. doi: 10.1016/j.soilbio.2005.08.020

Manze, U., Vogel, J., Streit, R., and Brunnacker, K. (1974). Isotopenuntersuchungen zum kalkumsatz im Löß. *Geol. Rundsch.* 63, 885–896.

McDonald, E. V., and Busacca, A. J. (1992). Late quaternary stratigraphy of loess in the channeled scabland and Palouse regions of Washington state. *Quat. Res.* 38, 141–156. doi: 10.1016/0033-5894(92)90052-K

Melander, L., and Saunders, W. H. (1979). *Reaction Rates of Isotopic Molecules*. New York, NY: Wiley.

Meyer-Heintze, S., Sprafke, T., Schulte, P., Terhorst, B., Lomax, J., Fuchs, M., et al. (2017). The MIS 3/2 transition in a new loess profile at Krems-Wachtberg East – A multi-methodological approach. *Quat. Int.* 464, 370–385. doi: 10.1016/j.quaint.2017.11.048

Midwood, A. J., and Boutton, T. W. (1998). Soil carbonate decomposition by acid has little effect on δ13C of organic matter. *Soil Biol. Biochem.* 30, 1301–1307. doi: 10.1016/s0038-0717(98)00030-3

Moine, O., Antoine, P., Hatté, C., Landais, A., Mathieu, J., Prud'homme, C., et al. (2017). The impact of last glacial climate variability in west-European loess revealed by radiocarbon dating of fossil earthworm granules. *Proc. Natl. Acad. Sci. U.S.A.* 24, 6209–6214. doi: 10.1073/pnas.1614751114

Moinet, G. Y. K., Hunt, J. E., Kirschbaum, M. U. F., Morcom, C. P., Midwood, A. J., and Millard, P. (2018). The temperature sensitivity of soil organic matter decomposition is constrained by microbial access to substrates. *Soil Biol. Biochem.* 116, 333–339. doi: 10.1016/j.soilbio.2017.10.031

Nettleton, W. D., Brasher, B. R., Benham, E. C., and Ahrenst, R. J. (1998). A classification system for buried palaeosols. *Quat. Int.* 51, 175–183. doi: 10.1016/s1040-6182(97)00043-8

Nettleton, W. D., Olson, C. G., and Wysocki, D. A. (2000). Paleosol classification: problems and solutions. *Catena* 41, 61–92. doi: 10.1016/s0341-8162(00)00109-0

Nordt, L. C., Hallmark, C. T., Wilding, L. P., and Boutton, T. W. (1998). Quantifying pedogenic carbonate accumulations using stable carbon isotopes. *Geoderma* 82, 115–136. doi: 10.1016/s0016-7061(97)00099-2

Obreht, I., Buggle, B., Catto, N., Markovic, S., Bösel, S., Vandenberghe, D., et al. (2014). The late Pleistocene Belotinac section (southern Serbia) at the southern limit of the European loess belt: environmental and climate reconstruction using grain size and stable C and N isotopes. *Quat. Int.* 334–335, 10–19. doi: 10.1016/j.quaint.2013.05.037

O'Leary, M. H. (1981). Carbon isotope fractionation in plants. *Phytochemistry* 20, 553–567. doi: 10.1016/0031-9422(81)85134-5

O'Leary, M. H. (1988). Carbon isotopes in photosynthesis. *Bioscience* 38, 328–336. doi: 10.2307/131073

Pécsi, M. (1990). Loess is not just the accumulation of dust. *Quat. Int.* 7–8, 1–21. doi: 10.1016/1040-6182(90)90034-2

Pirasteh-Anosheh, H., Saed-Moucheshi, A., Pakniyat, H., and Pessarakli, M. (2016). "Stomatal responses to drought stress," in *Water Stress and Crop Plants: A Sustainable Approach*, ed. P. Ahmad (Hoboken, NJ: Wiley), 24–35.

Profe, J., Zolitschka, B., Schirmer, W., Frechen, M., and Ohlendorf, C. (2016). Geochemistry unravels MIS 3/2 paleoenvironmental dynamics at the loess–paleosol sequence Schwalbenberg II, Germany. *Palaeogeogr. Palaeoclimatol. Palaeoecol.* 459, 537–551. doi: 10.1016/j.palaeo.2016.07.022

Prud'homme, C., Lécuyer, C., Antoine, P., Hatté, C., Moine, O., Fourel, F., et al. (2018). δ 13 C signal of earthworm calcite granules: a new proxy for palaeoprecipitation reconstructions during the last glacial in Western Europe. *Quat. Sci. Rev.* 179, 158–166. doi: 10.1016/j.quascirev.2017.11.017

Pye, K., and Tsoar, H. (2009). *Aeolian Sand and Sand Dunes*. Berlin: Springer.

Quade, J., Cerling, T. E., and Bowman, J. R. (1989). Systematic variations in carbon and oxygen isotopic composition of pedogenic carbonate along elevation transects in the southern Great Basin, United States. *Geol. Soc. Am. Bull.* 101, 464–475. doi: 10.1130/0016-7606(1989)101<0464:svitca>2.3.co;2

Rasmussen, S. O., Bigler, M., Blockley, S. P., Blunier, T., Buchardt, S. L., Clausen, H. B., et al. (2014). A stratigraphic framework for abrupt climatic changes during the last glacial period based on three synchronized Greenland ice-core records: refining and extending the INTIMATE event stratigraphy. *Quat. Sci. Rev.* 106, 14–28. doi: 10.1016/j.quascirev.2014.09.007

Reyes, F. R., and Lougheed, V. L. (2015). Rapid nutrient release from permafrost thaw in arctic aquatic ecosystems. *Arct. Antarct. Alp. Res.* 47, 35–48. doi: 10.1657/AAAR0013-099

Rousseau, D. D., Boers, N., Sima, A., Svensson, A., Bigler, M., Lagroix, F., et al. (2017). (MIS3 & 2) millennial oscillations in Greenland dust and Eurasian Aeolian records – A paleosol perspective. *Quat. Sci. Rev.* 169, 99–113. doi: 10.1016/j.quascirev.2017.05.020

Ruth, U., Wagenbach, D., Steffensen, J. P., and Bigler, M. (2003). Continuous record of microparticle concentration and size distribution in the central Greenland NGRIP ice core during the last glacial period. *J. Geophys. Res.* 108, 1–12. doi: 10.1029/2002JD002376

Salomons, W., and Mook, W. G. (1976). Isotope geochemistry of carbonate dissolution and reprecipitation in soils. *Soil Sci.* 122, 15–24. doi: 10.1097/00010694-197607000-00003

Schirmer, W. (2012). Rhine loess at schwalbenberg II - MIS 4 and 3. *Eiszeitalter Ggw.* 61, 32–47. doi: 10.3285/eg.61.1.03

Schirmer, W. (2013). *Ahrgau-Subformation. Lithostratigraphisches Lexikon*. Hannover: BGR.

Schirmer, W. (2016). Late Pleistocene loess of the lower Rhine. *Quat. Int.* 411, 44–61. doi: 10.1016/j.quaint.2016.01.034

Schirmer, W., Ikinger, A., and Nehring, F. (2012). Die terrestrischen Böden im Profil schwalbenberg/Mittelrhein. *Mainzer Geowissensch. Mitt.* 40, 53–78.

Sirocko, F., Knapp, H., Dreher, F., Förster, M. W., Albert, J., Brunck, H., et al. (2016). Reconstruction of landscape evolution zones (LEZ) from laminated Eifel maar sediments of the last 60,000 years. *Glob. Planet. Change* 142, 108–135. doi: 10.1016/j.gloplacha.2016.03.005

Sprafke, T., and Obreht, I. (2016). Loess: rock, sediment or soil – What is missing for its definition? *Quat. Int.* 399, 198–207. doi: 10.1016/j.quaint.2015.03.033

Stevenson, B. A., Kelly, E. F., McDonald, E. V., and Busacca, A. J. (2005). The stable carbon isotope composition of soil organic carbon and pedogenic carbonates along a bioclimatic gradient in the Palouse region, Washington State, USA. *Geoderma* 124, 37–47. doi: 10.1016/j.geoderma.2004.03.006

Thornton, B., Martin, G., Procee, M., Miller, D. R., Coull, M., Yao, H., et al. (2015). Distributions of carbon and nitrogen isotopes in Scotland's topsoil: a national-scale study: stable isotopes in Scotland's topsoil. *Eur. J. Soil Sci.* 66, 1002–1011. doi: 10.1111/ejss.12289

Vandenberghe, J. (2013). Grain size of fine-grained windblown sediment: a powerful proxy for process identification. *Earth Sci. Rev.* 121, 18–30. doi: 10.1016/j.earscirev.2013.03.001

von Lützow, M., and Kögel-Knabner, I. (2009). Temperature sensitivity of soil organic matter decomposition—what do we know? *Biol. Fertil. Soils* 46, 1–15. doi: 10.1007/s00374-009-0413-8

von Lützow, M., Kögel-Knabner, I., Ekschmitt, K., Matzner, E., Guggenberger, G., Marschner, B., et al. (2006). Stabilization of organic matter in temperate soils: mechanisms and their relevance under different soil conditions - a review. *Eur. J. Soil Sci.* 57, 426–445. doi: 10.1111/j.1365-2389.2006.00809.x

Wang, D., and Anderson, D. W. (2000). Pedogenic carbonate in Chernozemic soils and landscapes of southeastern Saskatchewan. *Can. J. Soil Sci.* 80, 251–261. doi: 10.4141/S99-063

Wardle, D. A. (1992). A comparative assessment of factors which influence microbial biomass carbon and nitrogen levels in soil. *Biol. Rev.* 67, 321–358. doi: 10.1111/j.1469-185X.1992.tb00728.x

Weninger, B., and Jöris, O. (2008). A 14C age calibration curve for the last 60 ka: the Greenland-Hulu U/Th timescale and its impact on understanding the Middle to Upper Paleolithic transition in Western Eurasia. *J. Hum. Evol.* 55, 772–781. doi: 10.1016/j.jhevol.2008.08.017

West, L. T., Wilding, L. P., and Hallmark, C. T. (1988). Calciustolls in central Texas: II. Genesis of calcic and petrocalcic horizons. *Soil Sci. Soc. Am. J.* 52, 1731–1740. doi: 10.2136/sssaj1988.03615995005200060040x

Yakir, D., and Israeli, Y. (1995). Reduced solar irradiance effects on net primary productivity (NPP) and the δ13C and δ18O values in plantations of *Musa* sp., *Musaceae*. *Geochim. Cosmochim. Acta* 59, 2149–2151. doi: 10.1016/s0016-7037(99)80010-6

Zamanian, K., Pustovoytov, K., and Kuzyakov, Y. (2016). Pedogenic carbonates: forms and formation processes. *Earth Sci. Rev.* 157, 1–17. doi: 10.1016/j.earscirev.2016.03.003

Zech, M., Zech, R., and Glaser, B. (2007). A 240,000-year stable carbon and nitrogen isotope record from a loess-like palaeosol sequence in the Tumara Valley, Northeast Siberia. *Chem. Geol.* 242, 307–318. doi: 10.1016/j.chemgeo.2007.04.002

Zens, J., Zeeden, C., Römer, W., Fuchs, M., Klasen, N., and Lehmkuhl, F. (2017). The Eltville Tephra (Western Europe) age revised: integrating stratigraphic and dating information from different last glacial loess localities. *Palaeogeogr. Palaeoclimatol. Palaeoecol.* 466, 240–251. doi: 10.1016/j.palaeo.2016.11.033

Zerboni, A., Trombino, L., and Cremaschi, M. (2011). Micromorphological approach to polycyclic pedogenesis on the Messak Settafet plateau (central Sahara): formative processes and palaeoenvironmental significance. *Geomorphology* 125, 319–335. doi: 10.1016/j.geomorph.2010.10.015

Zheng, S., and Shangguan, Z. (2007). Spatial patterns of leaf nutrient traits of the plants in the Loess Plateau of China. *Trees* 21, 357–370. doi: 10.1007/s00468-007-0129-z

Conflict of Interest: The authors declare that the research was conducted in the absence of any commercial or financial relationships that could be construed as a potential conflict of interest.